

The *Gaia* Ultra-Cool Dwarf Sample – III: Seven new multiple systems containing at least one *Gaia* DR2 ultra-cool dwarf.

F. Marocco^{1,2*} †, R. L. Smart³, E. E. Mamajek¹, L. M. Sarro⁴, A. J. Burgasser⁵, J. A. Caballero⁶, J. M. Rees⁵, D. Caselden⁷, K. L. Cruz^{8,9,10}, R. Van Linge⁵, D. J. Pinfield¹¹

¹Jet Propulsion Laboratory, California Institute of Technology, 4800 Oak Grove Dr., Pasadena, CA 91109, USA

²IPAC, Mail Code 100-22, California Institute of Technology, 1200 E. California Blvd., Pasadena, CA 91125, USA

³Istituto Nazionale di Astrofisica, Osservatorio Astrofisico di Torino, Strada Osservatorio 20, I-10025 Pino Torinese, Italy

⁴Department of Artificial Intelligence, Universidad Nacional de Educación a Distancia, c/ Juan del Rosal 16, E-28040 Madrid, Spain

⁵Center for Astrophysics and Space Science, University of California San Diego, La Jolla, CA 92093, USA

⁶Centro de Astrobiología (CSIC-INTA), ESAC, Camino Bajo del Castillo s/n, E-28692 Villanueva de la Cañada, Madrid, Spain

⁷Gigamon Applied Threat Research, 619 Western Avenue, Suite 200, Seattle, WA 98104, USA

⁸Department of Physics and Astronomy, Hunter College, City University of New York, 695 Park Avenue, New York, NY 10065, USA

⁹Physics, Graduate Center of the City University of New York, 365 5th Avenue, New York, NY 10016, USA

¹⁰Department of Astrophysics, American Museum of Natural History, Central Park West at 79th Street, New York, NY 10024, USA

¹¹Centre for Astrophysics Research, School of Physics, Astronomy and Mathematics, University of Hertfordshire, College Lane, Hatfield AL10 9AB, UK

Accepted 2020 April 7. Received 2020 April 6; in original form 2019 September 26

ABSTRACT

We present ten new ultra-cool dwarfs in seven wide binary systems discovered using *Gaia* DR2 data, identified as part of our *Gaia* Ultra-Cool Dwarf Sample project. The seven systems presented here include an L1 companion to the G5 IV star HD 164507, an L1: companion to the V478 Lyr AB system, an L2 companion to the metal-poor K5 V star CD-28 8692, an M9 V companion to the young variable K0 V star LT UMa, and three low-mass binaries consisting of late Ms and early Ls. The HD 164507, CD-28 8692, V478 Lyr, and LT UMa systems are particularly important benchmarks, because the primaries are well characterised and offer excellent constraints on the atmospheric parameters and ages of the companions. We find that the M8 V star 2MASS J23253550+4608163 is ~ 2.5 mag overluminous compared to M dwarfs of similar spectral type, but at the same time it does not exhibit obvious peculiarities in its near-infrared spectrum. Its overluminosity cannot be explained by unresolved binarity alone. Finally, we present an L1+L2 system with a projected physical separation of 959 au, making this the widest L+L binary currently known.

Key words: binaries: visual – stars: low-mass – brown dwarfs – stars: individual: HD 164507, V478 Lyr, CD-28 8692, LT UMa

1 INTRODUCTION

Ultra-cool dwarfs (UCDs, spectral type $\geq M7$) in binary systems with main sequence and post-main sequence stars are valuable benchmarks (Pinfield et al. 2006), providing robust tests of ultra-cool atmospheric and evolutionary models. Under the reasonable assumption of common origin, a bright

main sequence primary provides constraints on the metallicity and the age of a system, two parameters that are currently difficult to infer for isolated ultra-cool dwarfs.

UCDs are a mixture of the lowest mass hydrogen fusing stars and sub-stellar non-hydrogen-fusing objects. Mass, age, metallicity, and luminosity are degenerate parameters for these objects, and the presence (and evolution) of dust clouds in the photosphere further complicates the interpretation of their spectra (Burrows et al. 2006; Saumon & Marley 2008). Furthermore sub-stellar UCDs overlap in both mass

* NASA Postdoctoral Program Fellow

† E-mail: federico.marocco@jpl.nasa.gov

and temperature with the gaseous giant planets in exosolar systems (e.g. [Faherty et al. 2016](#)), but can be studied without the additional complication of the planets' vicinity to a bright host star. A full understanding of ultra-cool atmospheres is therefore of vital importance if we wish to understand exoplanets and their formation and evolution.

The recent second data release from the ESA mission *Gaia* ([Gaia Collaboration et al. 2016a, 2018](#)) provides exquisite astrometry for ~ 1.3 billion objects within our Galaxy ([Lindgren et al. 2018](#)), allowing access to a huge population of wide binaries consisting of an ultra-cool dwarf in a system with a star or white dwarf ([Marocco et al. 2017](#)). In particular, the greatly increased volume probed by *Gaia*, and the resulting increased pool of potential primary stars, offers for the first time the possibility to map the full age–temperature–metallicity parameter space, large regions of which are currently undersampled or completely unexplored (see e.g. [Day-Jones et al. 2011](#); [Deacon et al. 2014](#); [Marocco et al. 2017](#)). While the advent of *Gaia* expands the pool of potential primaries, existing optical and near-infrared surveys, and the astrometric catalogues that spawned from them (e.g. ULAS, [Smith et al. 2014](#); VIRAC, [Smith et al. 2018](#); CatWISE, [Eisenhardt et al. 2019](#)), grant access to a vast population of ultra-cool dwarfs across spectral types M, L, T, and Y. We have therefore set out to complete the nearby census of these objects, to fully explore and characterise ultra-cool atmospheres.

In this paper we present seven new multiple systems containing at least one *Gaia* DR2 ultra-cool dwarf component.

In Section 2 we describe our candidate selection; in Section 3 we summarise observing and data reduction procedures; in Section 4 we discuss in more detail the newly discovered systems; in Section 5 we compare the main features in the spectra of the new UCDs; finally in Section 6 we summarise our findings and discuss future work.

2 CANDIDATE SELECTION

We identified an initial list of 8013 UCD candidates from the *Gaia* DR2 catalogue as follows. First, we queried the catalogue for *Gaia* sources fainter than the maximum brightness that an UCD at the measured parallax could have, as predicted by the BT-Settl models ([Allard et al. 2012a, 2013](#)). The maximum distance is 373 pc, the distance at which the brightest, hottest UCD ($T_{\text{eff}} \sim 2500$ K) would be fainter than the *Gaia* limiting magnitude ($G = 20.7$ mag). We required the $G - G_{\text{RP}}$ colour to be redder than 1.4 mag (since UCDs are typically redder than that; [Smart et al. 2017, 2019](#)). To minimise the number of sources with spurious astrometric measurements, we removed candidates within 5 degrees of the Galactic plane and inside an ellipse centred at the Galactic centre with semi-major axis along the Galactic longitude axis of 50° , and 8° along the Galactic latitude axis. To retain only reliable astrometric measurements, we required sources to have more than six visibility periods and astrometric excess noise lower than 5 mas. We computed posterior probability densities of the distance given the parallax measurements and associated uncertainties using an exponentially decreasing constant volume density prior, and selected sources with a posterior probability to be within

373 pc greater than 0.5. We then fit a principal curve ([Hastie & Stuetzle 1989](#)) in the M_G versus $G - G_{\text{RP}}$ plane to the values of the resulting set, and calibrated the curve in effective temperature using the spectral types of sources in the *Gaia* Ultra-Cool Dwarfs Sample ([Smart et al. 2017, 2019](#)) and the [Stephens et al. \(2009\)](#) conversion between spectral types and effective temperatures. Finally, we computed the projections of the UCD candidate positions in the M_G versus G_{RP} plane along the principal curve and assigned effective temperatures accordingly. A cut at $T_{\text{eff}} \leq 2500$ K resulted in the 8013 candidates mentioned above.

We searched for binaries among these 8013 UCD candidates using the criteria defined in [Smart et al. \(2019, hereafter GUCDS II\)](#):

$$\begin{aligned} \rho &< 100 \varpi \\ \Delta\varpi &< \max[3\sigma_\varpi, 1 \text{ mas}] \\ \Delta\mu &< 0.1 \mu \\ \Delta\theta &< 15^\circ, \end{aligned} \tag{1}$$

where ρ is the separation on the sky in arcseconds, $\Delta\varpi$ is the difference between the candidate UCD and primary parallax, ϖ and σ_ϖ are the parallax and parallax uncertainty for the UCD (in mas), $\Delta\mu$ is the difference of the total proper motions, and $\Delta\theta$ is the difference of the position angles. The maximum ρ was chosen to correspond to 100,000 au as a conservative upper limit for the projected physical separation (s). This separation meets the binding energy criterion of $|U_g^*| > 10^{33} J$ as developed by [Caballero \(2009\)](#) for a system of a 0.1 and a 2 M_\odot objects. The parallax criterion is a compromise between a standard 3σ criterion, and a more conservative 1.0 mas difference to allow for parallaxes that had unrealistically low errors. For the proper motion, using a standard 3σ criterion would remove nearby objects with significant orbital motion, so we choose a conservative 10% agreement, which is large enough to accommodate most orbital motions but small enough to reduce false positives. As discussed in GUCDS II these criteria fail for the nearby binary systems GJ 1048 A/B and G 239-25 A/B (in both cases because the modulus of the proper motions differs by more than 10%). Therefore, our catalogue of binary candidates should not be regarded as complete.

Of the 8013 UCD candidates, 840 have a possible companion according to the criteria above. The seven systems presented here are those that we could observe during our observing nights at the Palomar Observatory. We present their astrometric properties and spectral types in Tables 1 and 2. We collected optical and near-infrared photometry for both components of our newly discovered systems from *Gaia* DR2, 2MASS ([Skrutskie et al. 2006](#)), PanSTARRS DR1 ([Chambers et al. 2016](#)), and AllWISE ([Cutri et al. 2013](#)). The photometry is also presented in Tables 1 and 2. In Figure 1 we show a colour-magnitude diagram based on *Gaia* colours and astrometry. The small grey points are objects in *Gaia* DR2 nominally within 50 pc, selected using Equation C.1 and C.2 from [Lindgren et al. \(2018\)](#). Red points are UCDs identified in *Gaia* DR2 by GUCDS II. The position of the seven systems presented here is highlighted with different symbols, with the primary plotted in blue and the companion in green. Two objects stand out at first glance: HD 164507 B, and 2MASS J23253550+4608163. We will discuss their properties in Sections 4.1 and 4.4.

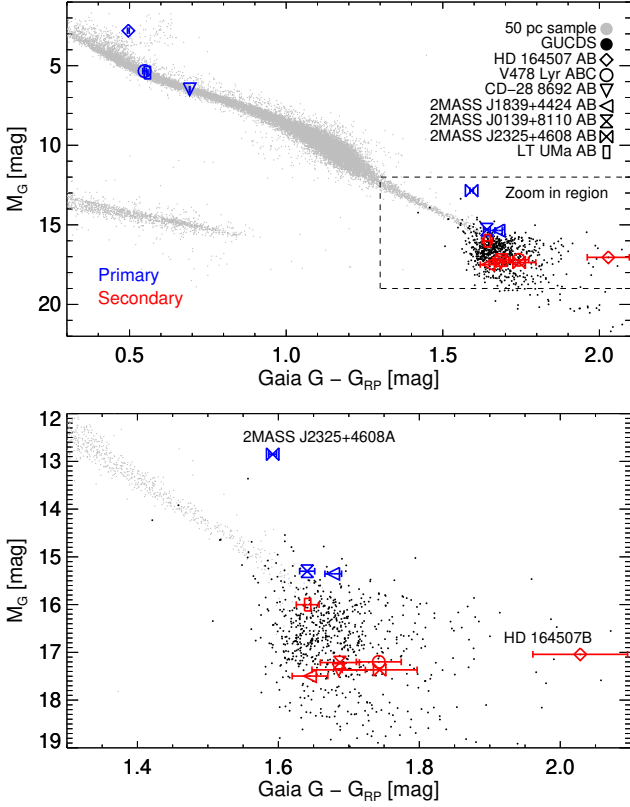


Figure 1. Colour-magnitude diagrams depicting the full stellar sequence (top) and a zoom into the ultra-cool dwarfs region (bottom). The small grey points are stars in *Gaia* DR2 nominally within 50 pc, selected using the criteria described in Appendix C of Lindegren et al. (2018). Red points are the ultra-cool dwarfs identified in *Gaia* DR2 by GUCDS II. The seven systems presented here are plotted with different symbols, with the primary in each system plotted in blue and the companion in green. Vertical error bars are typically smaller than the symbols. Detailed analysis of individual systems can be found in Section 4.

Table 1. Astrometry, photometry, and spectral types for the HD 164507 AB, V478 Lyr ABC, CD-28 8692 AB, and 2MASS J1839+4424 AB systems.

	HD 164507		V478 Lyr		CD-28 8692		2MASS J1839+4424	
	A	B	AB	C	A	B	A	B
R.A. (hh:mm:ss.ss)	18:00:57.22	18:00:58.48	19:07:32.52	19:07:33.23	11:10:25.97	11:10:29.21	18:39:29.22	18:39:27.40
Dec. (dd:mm:ss.s)	+15:05:35.3	+15:05:18.3	+30:15:17.8	+30:15:32.1	-29:24:51.5	-29:25:19.8	+44:24:41.2	+44:24:51.0
Sep. (arcsec)	25.01		17.05		50.91		21.89	
Sep. (au)	1136		462		2026		811	
P.A. (deg)	132.58		32.63		123.84		296.62	
Sp. type	G5 IV ¹	L1	G8 V SB ²	L1:	K5 V ³	L2	M9 V ⁴	L2
ϖ (mas)	22.009 ± 0.037	24.8 ± 1.4	36.877 ± 0.026	37.02 ± 0.46	25.133 ± 0.042	24.68 ± 0.97	27.00 ± 0.41	27.01 ± 0.70
$\mu_\alpha \cos \delta$ (mas yr ⁻¹)	-53.138 ± 0.068	-57.6 ± 1.5	110.850 ± 0.040	112.39 ± 0.62	-9.948 ± 0.064	-10.9 ± 1.6	20.01 ± 0.75	29.3 ± 1.5
μ_δ (mas yr ⁻¹)	-98.328 ± 0.095	-95.2 ± 1.4	103.117 ± 0.045	103.47 ± 0.91	-74.913 ± 0.059	-73.2 ± 1.4	171.09 ± 0.77	173.0 ± 2.5
<i>Gaia</i> <i>G</i> (mag)	6.08969 ± 0.00046	20.070 ± 0.013	7.5035 ± 0.0016	19.3571 ± 0.0045	9.48280 ± 0.00018	20.4050 ± 0.0077	18.1977 ± 0.0042	20.3391 ± 0.0083
<i>Gaia</i> <i>G_{RP}</i> (mag)	5.5936 ± 0.0028	18.041 ± 0.066	6.9557 ± 0.0054	17.615 ± 0.032	8.79104 ± 0.00078	18.719 ± 0.037	16.520 ± 0.011	18.694 ± 0.024
PS1 <i>r</i> (mag)	7.7177 ± 0.0095	...	9.507 ± 0.064	21.14 ± 0.19	20.334 ± 0.015	21.693 ± 0.044
PS1 <i>i</i> (mag)	...	18.81 ± 0.17	7.73 ± 0.22	18.474 ± 0.014	9.50 ± 0.24	19.959 ± 0.024	17.6724 ± 0.0027	19.8205 ± 0.0077
PS1 <i>z</i> (mag)	...	17.779 ± 0.029	7.4026 ± 0.0063	17.37 ± 0.14	9.848 ± 0.021	18.456 ± 0.013	16.2113 ± 0.0034	18.4309 ± 0.0076
PS1 <i>y</i> (mag)	...	16.302 ± 0.058	6.817 ± 0.022	16.1001 ± 0.0060	8.8370 ± 0.0010	17.482 ± 0.019	15.3240 ± 0.0043	17.4922 ± 0.0083
2MASS <i>J</i> (mag)	5.19 ± 0.26	15.416 ± 0.051 ^c	6.232 ± 0.020	> 13.663	7.922 ± 0.019	15.421 ± 0.062	13.433 ± 0.029	15.432 ± 0.054
2MASS <i>H</i> (mag)	4.700 ± 0.053	14.755 ± 0.082 ^c	5.855 ± 0.016	> 13.210	7.414 ± 0.044	14.535 ± 0.046	12.792 ± 0.035	14.598 ± 0.059
2MASS <i>K_s</i> (mag)	4.551 ± 0.020	14.142 ± 0.067 ^c	5.741 ± 0.020	13.021 ± 0.042 ^c	7.276 ± 0.018	14.085 ± 0.076	12.356 ± 0.028	13.901 ± 0.047
AllWISE <i>W1</i> (mag)	4.56 ± 0.20 ^b	11.007 ± 0.021 ^d	5.76 ± 0.12 ^b	...	7.123 ± 0.035 ^b	13.641 ± 0.024 ^a	12.002 ± 0.023	13.540 ± 0.026
AllWISE <i>W2</i> (mag)	4.417 ± 0.056 ^b	10.884 ± 0.021 ^d	5.580 ± 0.045 ^b	...	7.298 ± 0.019	13.406 ± 0.029 ^a	11.750 ± 0.022	13.291 ± 0.028
AllWISE <i>W3</i> (mag)	4.569 ± 0.015 ^b	10.666 ± 0.092 ^d	5.667 ± 0.015 ^b	...	7.255 ± 0.017	> 12.581	11.29 ± 0.10	12.60 ± 0.36

Notes: Coordinates, parallax and proper motion are from *Gaia* DR2. Separation and position angle are computed at the *Gaia* DR2 epoch (2015.5). Spectral types are assigned using SPLAT (see Section 3), except for HD 164507, V478 Lyr AB, CD-28 8692, and 2MASS J18392917+4424386, whose spectral types are taken from the literature. References: 1-Harlan & Taylor (1970); 2-Fekel (1988); 3-Uppgren et al. (1972); 4-Bardalez Gagliuffi et al. (2014). Notes on photometry: ^acontaminated by bright star halo; ^bsaturated; ^ccontaminated by bright star; ^dcontaminated by diffraction spike.

3 OBSERVATIONS

We obtained near-infrared spectra for the ultra-cool dwarfs in our newly discovered binary systems using TripleSpec on the 200" telescope at the Palomar Observatory on 2018 April 27-29, 2018 October 16 and 18, and 2019 April 16 (Proposals 2018A J12, 2018B J08, and 2019A J14; PI: Mamajek; see Appendix A). TripleSpec is a near-infrared echelle spectrograph, that delivers a resolution of 2500–2700 over the wavelength range 1.0 – 2.4 μ m (Herter et al. 2008).

Targets were observed following a standard ABBA nodding pattern with a nod throw of 11 arcsec. The slit was aligned to the parallactic angle to minimise atmospheric distortion, with the exceptions of HD 164507 B, V478 Lyr C, and 2MASS J232535.09+460809.3, for which we rotated the slit to avoid the bright primary. We observed an A0 V star (selected using the Gemini Telluric Standard Search on-line tool¹) for telluric correction after each target, matching the airmass of observation as closely as possible.

The data were reduced using a modified version of the IDL package *Spextool* (Cushing et al. 2004). The program applies basic calibration (dark subtraction and flat fielding), then pair-wise subtracts the images to remove sky background. The individual orders of the echelle spectra are traced and extracted, and wavelength calibration is achieved using the numerous OH sky lines. The individual orders are corrected for telluric absorption and flux calibrated using the observed telluric standard star, chosen to match the Vega spectrum used as template in *Spextool*. The individual orders are then merged, using their overlap to determine flux adjustments when needed. The reduced spectra are presented in Figures 2, 3, and 4.

We assigned a spectral type to our targets via standard template-matching using the *classifyByStandard* routine in the PYTHON package *SPLAT*² (Burgasser et al. 2016). The code interpolates the templates to the same wavelength grid of the observed spectra, and then minimises the χ^2 of the fit, treating the scaling between the flux-calibrated target and the normalised templates as a free parameter of the fit. The *classifyByStandard* routine offers the possibility to classify objects by fitting the full spectrum, as well as by fitting only the *J* band, following the prescriptions of Kirkpatrick et al. (2010). The spectral types obtained with the two methods agree to within ± 1 subtype, with the exception of CD-28 8692 B and 2MASS J0139+8110 A. We discuss the discrepancies and our adopted classification in Section 4.3 and 4.5. We used the standard M, L, and T templates defined in Burgasser et al. (2006) and Kirkpatrick et al. (2010), except in the case of V478 Lyr C, where standard templates gave poor fits. Further details on the spectral typing for this source are given in Section 4.2. The results from template matching are presented in Figures 2, 3, and 4, and the assigned spectral types are listed in Tables 1 and 2.

¹ <https://www.gemini.edu/sciops/instruments/nearir-resources/spectroscopic-standards-telluric-standard-search>

² <http://pono.ucsd.edu/~adam/browndwarfs/splat>

4 NOTES ON INDIVIDUAL SYSTEMS

4.1 HD 164507 AB

The primary is a very well characterised G5IV star that is included in the catalogue of radial velocity standards for *Gaia* (Soubiran et al. 2013). Several independent estimates of the atmospheric and evolutionary parameters for this sub-giant can be found in the literature, and here we briefly summarise those based on high-resolution spectroscopy only.

Valenti & Fischer (2005) obtained $R \sim 70,000$ spectroscopy for HD 164507 using the High-Resolution Echelle Spectrometer (HIRES) on the 10 m telescope at Keck Observatory (Vogt et al. 1994). They derived atmospheric parameters using version 2.1 of the software package Spectroscopy Made Easy (SME; Valenti & Piskunov 1996) and the atmospheric models by Kurucz (1992). Mass and age for the star were then derived using the Y^2 isochrones (Demarque et al. 2004). Takeda et al. (2007) and Maldonado et al. (2013) derived independent age and mass using the atmospheric parameters from Valenti & Fischer (2005). Takeda et al. (2007) employed the Yale Rotational Evolution Code (YREC) in its non-rotating mode (Demarque et al. 2008) to generate their set of isochrones, while Maldonado et al. (2013) used the Valenti & Fischer (2005) spectroscopic T_{eff} and metallicity together with *Hipparcos* data as inputs for PARAM³ (da Silva et al. 2006) to derive age and mass for HD 164507.

Jofré et al. (2015) used high-resolution spectroscopy from SOPHIE on the 1.93 m telescope at the Observatoire de Haute-Provence (Perruchot et al. 2008). The fundamental stellar parameters (T_{eff} , $\log g$, [Fe/H], ξ_t) were computed homogeneously using the FUNDPAR code (Saffe 2011). The chemical abundances of 14 elements (Na, Mg, Al, Si, Ca, Sc, Ti, V, Cr, Mn, Co, Ni, Zn, and Ba) were obtained using the 2009 version of the MOOG⁴ code (Snedden 1973). Rotational velocities were derived from the full width at half maximum of isolated Fe lines. Again, mass and age were derived using PARAM.

Niedzielski et al. (2016) used the High Resolution Spectrograph (Tull 1998) on the Hobby-Eberly Telescope. The T_{eff} , $\log g$, ξ_t , and [Fe/H] were obtained from the measured equivalent width of neutral and ionised iron absorption lines, with the TGVIT code (Takeda et al. 2002, 2005). The stellar mass and age were determined using a Bayesian method described in Adamczyk et al. (2016), with theoretical stellar models from Bressan et al. (2012). Deka-Szymankiewicz et al. (2018) updated the age and mass derived by Niedzielski et al. (2016) using the *Gaia* DR2 parallax.

Luck (2017) used spectra from The McDonald Observatory 2.1 m Telescope and Sandiford Cassegrain Echelle Spectrograph (McCarthy et al. 1993). Abundances and ξ_t were calculated using measured equivalent widths and plane-parallel MARCS model atmospheres (Gustafsson et al. 2008), while T_{eff} and $\log g$ were computed from broad-band photometry and the photometric calibration of Casagrande et al. (2010). Finally, Luck (2017) determined mass and age using various sets of isochrones from Bertelli et al. (1994), Demarque et al. (2004), Dotter et al. (2008), and the 2016 version of the BaSTI isochrones (Pietrinferni et al. 2004).

³ http://stev.oapd.inaf.it/cgi-bin/param_1.1

⁴ <https://www.as.utexas.edu/~chris/moog.html>

Table 2. Astrometry, photometry, and spectral types for the 2MASS J0139+8110 AB, 2MASS J2325+4608 AB, and LT UMa AB systems presented here.

	2MASS J0139+8110		2MASS J2325+4608		LT UMa	
	A	B	A	B	A	B
R.A. (hh:mm:ss.ss)	01:39:09.00	01:38:59.67	23:25:35.40	23:25:35.09	08:44:47.95	08:44:50.12
Dec. (dd:mm:ss.s)	+81:09:59.7	+81:10:07.9	+46:08:15.8	+46:08:09.2	+55:32:19.7	+55:32:12.3
Sep. (arcsec)		23.00		7.24		19.83
Sep. (au)		959		378		879
P.A. (deg)		290.87		205.89		111.89
Sp. type	L1	L2	M8 V	L2	K0 V	M9 V
ϖ (mas)	23.98 ± 0.23	24.74 ± 0.79	19.13 ± 0.48	20.3 ± 1.4	22.550 ± 0.033	22.00 ± 0.43
$\mu_\alpha \cos \delta$ (mas yr ⁻¹)	-4.25 ± 0.51	-5.3 ± 1.4	-52.19 ± 0.64	-61.2 ± 2.6	76.636 ± 0.053	77.90 ± 0.60
μ_δ (mas yr ⁻¹)	-26.61 ± 0.33	-26.8 ± 1.0	-34.00 ± 0.51	-40.4 ± 1.8	12.890 ± 0.050	14.88 ± 0.57
<i>Gaia</i> <i>G</i>	18.4012 ± 0.0023	20.2468 ± 0.0070	16.4411 ± 0.0039	20.829 ± 0.012	8.6719 ± 0.0006	19.2895 ± 0.0033
<i>Gaia</i> <i>G_{RP}</i>	16.760 ± 0.010	18.560 ± 0.027	14.8492 ± 0.0038	19.086 ± 0.052	8.1151 ± 0.0020	17.648 ± 0.016
PS1 <i>r</i>	20.473 ± 0.046	> 20.031	17.7361 ± 0.0088	> 21.68	7.003 ± 0.001	> 17.26
PS1 <i>i</i>	17.801 ± 0.013	19.763 ± 0.066	15.6181 ± 0.0035	20.301 ± 0.027	9.149 ± 0.030	18.616 ± 0.028
PS1 <i>z</i>	16.4260 ± 0.0077	18.325 ± 0.020	14.6096 ± 0.0040	18.847 ± 0.016	...	17.231 ± 0.013
PS1 <i>y</i>	15.6106 ± 0.0067	17.327 ± 0.017	14.0252 ± 0.0029	17.806 ± 0.019	9.475 ± 0.001	16.333 ± 0.018
2MASS <i>J</i>	13.891 ± 0.028	15.239 ± 0.046	12.561 ± 0.020	15.868 ± 0.070	7.458 ± 0.018	14.704 ± 0.035^c
2MASS <i>H</i>	13.233 ± 0.038	14.400 ± 0.049	11.955 ± 0.021	14.783 ± 0.059	7.124 ± 0.051	13.951 ± 0.043^c
2MASS <i>K_s</i>	12.829 ± 0.030	13.896 ± 0.053	11.573 ± 0.018	14.348 ± 0.076	7.016 ± 0.026	13.491 ± 0.024^c
AllWISE <i>W1</i>	12.381 ± 0.022	13.419 ± 0.024	11.387 ± 0.023	13.693 ± 0.080	6.927 ± 0.051^b	...
AllWISE <i>W2</i>	12.125 ± 0.023	13.109 ± 0.027	11.172 ± 0.021	13.493 ± 0.077	7.007 ± 0.020^b	...
AllWISE <i>W3</i>	11.64 ± 0.19	12.76 ± 0.46	10.90 ± 0.11	> 11.946	6.985 ± 0.017	...

Notes: Coordinates, parallax and proper motion are from *Gaia* DR2. Separation and position angle are computed at the *Gaia* DR2 epoch (2015.5). Spectral types are assigned using SPLAT (see Section 3), except for LT UMa A, whose spectral types is taken from Strassmeier et al. (2000). Notes on photometry: ^acontaminated by bright star halo; ^bsaturated; ^ccontaminated by bright star; ^dcontaminated by diffraction spike.

Finally, *Gaia* DR2 quotes $T_{\text{eff}} = 5560^{+115}_{-62}$ K (see Andrae et al. 2018, for details on how *Gaia* DR2 atmospheric parameters are derived), and the best-fit template used for radial velocity measurement has $T_{\text{eff}} = 5500$ K, $\log g = 3.5$, and $[\text{Fe}/\text{H}] = +0.2$ (Sartoretti et al. 2018), all in good agreement with the literature values.

The atmospheric parameters discussed above are listed in Table 3. The values derived are in general agreement with each other, and in particular point towards a slightly super solar metallicity ($[\text{Fe}/\text{H}] = 0.03 - 0.19$ dex), and an age for the system in the range 3.0 – 5.9 Gyr.

More accurate age constraints on this star will be provided by *TESS* (Ricker et al. 2015) via gyrochronology, making this system an exquisite benchmark for UCD models and retrieval codes testing (Line et al. 2015; Burningham et al. 2017, 2013).

The L1 companion, HD 164507 B, is an outlier in the colour-magnitude diagram of Figure 1. With a $G - G_{\text{RP}}$ colour of 2.028 ± 0.067 mag, it is among the reddest UCDs in the *Gaia* sample. Objects with similar $G - G_{\text{RP}}$ colour are found in GUCDS II to be either tight binaries or suspect tight binaries. The red $G - G_{\text{RP}}$ colour in this case would be due to the fact that G_{RP} (and G_{BP}) magnitudes are determined by integrating the G_{RP} fluxes in a 3.5×2.1 arcsec² window, and there is currently no treatment of multiple sources in the same window in *Gaia* DR2 (Evans et al. 2018). Therefore, an excess in G_{RP} for close binary systems is expected. However, there is no evidence for binarity of HD 164507 B. The source is not resolved by *Gaia*, and the goodness-of-fit and astrometric excess noise reported in *Gaia* DR2 (2.7359 and 2.108 mas, respectively) are both con-

sistent with the mean values for UCDs found in GUCDS II (5.2 ± 2.6 and 2.2 ± 1.2 mas, respectively). The primary has higher-than-solar metallicity ($0.03 < [\text{Fe}/\text{H}] < 0.19$ dex, see Section 4.1), and higher metallicity UCDs are expected to have redder than average colours because of the enhanced dust content in their photosphere (e.g. Looper et al. 2008; Marocco et al. 2014). However the near-infrared spectrum of HD 164507 B does not show obvious peculiarities (see Figure 2). Finally, youth is also typically associated with redder-than-usual colours (see e.g. Faherty et al. 2016), but young and suspected young objects in GUCDS II form a relatively tight sequence with $1.6 \lesssim G - G_{\text{RP}} \lesssim 1.8$ mag, and the age of the system rules out youth as a cause. Optical spectroscopy for this UCD is desirable to shed light on its nature.

We derive T_{eff} for the companion using the Filippazzo et al. (2015) spectral type to T_{eff} polynomial relation, and obtain $T_{\text{eff}} = 2100 \pm 29$ K. Linear interpolation of the BT-Settl isochrones⁵ for solar and super-solar metallicity ($[\text{Fe}/\text{H}] = +0.5$ dex) in the age range 3.0–5.9 Gyr, and for $T_{\text{eff}} = 2100 \pm 29$ K, gives a mass for the companion in the range 50–77 M_{Jup} , at or below the hydrogen burning limit.

To compute the bolometric luminosity (L_{bol}) we need to determine a bolometric correction, since our TripleSpec spectrum only covers the $1.0 < \lambda < 2.4 \mu\text{m}$ range. We did this by fitting the TripleSpec spectrum with the BT-Settl atmospheric models (Allard et al. 2012b) with the fitting technique developed by Cushing et al. (2008). The models

⁵ <https://phoenix.ens-lyon.fr/Grids/BT-Settl/CIFIST2011/ISOCHRONES/>

cover the T_{eff} space in steps of 50 K, the $\log g$ space in steps of 0.5 dex, and the $[\text{Fe}/\text{H}]$ space in steps of 0.5 dex.

We flux calibrated the target’s spectrum using the measured 2MASS J -band magnitude, and then allowed the scaling factor between the flux-calibrated spectrum and the models to be a parameter of the fit. The best fit scaling factor gave us a measurement of the radius (R) of the target via the simple geometric dilution factor $(R/d)^2$. We restricted the range of models to be considered for fitting to the ± 200 K range around the predicted T_{eff} of 2100 K and the metallicity to be within ± 0.5 dex of the metallicity of the primary, for which we chose the mid point of the values quoted in the literature, i.e. 0.11 dex.

We used the scaled best-fit atmospheric model to complete the TripleSpec spectrum at long and short wavelength ($\lambda < 1\mu\text{m}$ and $\lambda > 2.4\mu\text{m}$). L_{bol} was then computed by summing the flux density over the full model+TripleSpec spectrum, and multiplying it by $4\pi d^2$. The uncertainty on L_{bol} was computed by propagating the uncertainty on the measured spectrum, as well as the uncertainty on the 2MASS magnitude used for flux calibration, and the uncertainty on the distance.

The best fit model for HD 164507 B has $T_{\text{eff}} = 2300$ K, $\log g = 5.0$, and $[\text{Fe}/\text{H}] = +0.5$ dex. The radius corresponding to the best fit scale factor is $0.88 R_{\text{Jup}}$, and the bolometric luminosity is $\log_{10}(L_{\text{bol}}/L_{\odot}) = -3.144^{+0.039}_{-0.043}$. Approximately 17% of the bolometric luminosity reported here is outside of the TripleSpec wavelength range (1.0–2.4 μm). This fraction decreases with spectral type, as the contribution from the optical portion of the spectral energy distribution collapses, while the longer wavelength flux does not increase significantly. The model-dependent fraction of L_{bol} approaches $\sim 40\%$ for the late-Ms in our sample, and decreases down to $\sim 8\%$ for the L2s. The best fit model for HD 164507 B is shown in Figure 5. The overall fit is poor: (i) the model has a triangular H band, while the target has a much flatter H -band spectrum; (ii) the alkali lines in the J band are much too shallow in the model compared to the observed ones; (iii) the K -band spectrum in the model is too flat, and (iv) the overall spectrum is too blue compared to our target. The best fit T_{eff} is 200 K warmer than the prediction from the Filippazzo et al. (2015) polynomial.

4.2 V478 Lyr ABC

The primary is a chromospherically active G8 V single-lined spectroscopic binary with a period of about 2.13 d (Fekel 1988). This star was found to have strong ultraviolet emission features and a filled-in $H\alpha$ absorption line that is variable in strength. Therefore, Fekel (1988) classified it as an early-type BY Draconis system. The secondary had its mass estimated to be about $0.3 M_{\odot}$ and to be probably an M2–M3 dwarf. The inclination of the system was measured to be 67 ± 12 deg. The lithium abundance of the G8 dwarf, estimated from the equivalent width of the $\text{Li I } 6707.8 \text{ \AA}$ line (47 mÅ), led Fekel (1988) to propose an age for the system that is somewhat less than that of the Hyades cluster (680 Myr; Gossage et al. 2018).

Using the BANYAN Σ on-line tool, the *Gaia* DR2 astrometry, and the mean radial velocity from Nordström et al. (2004), we find a probability of 0% for the object to be a

member of any of the young moving groups considered in BANYAN Σ (including the Hyades).

Nevertheless, the UCD companion, dubbed V478 Lyr C, shows a somewhat triangular H -band spectrum, a feature previously associated with youth (Lucas et al. 2001; Allers & Liu 2013). Gravity-sensitive spectral indices and pseudo-equivalent width defined in Allers & Liu (2013) however lead to a L1 field surface gravity (FLD-G) classification for the companion. Intermediate surface gravity (INT-G) and very-low surface gravity (VL-G) objects in the Allers & Liu (2013) sample have typical age < 200 Myr and, according to a more recent study conducted by Martin et al. (2017), the reliability of the gravity classification drops significantly for objects with age > 100 Myr. On the other hand, the L1 companion to the young A3V star β Circini has a flat H -band spectrum (and no low gravity features, see Smith et al. 2015). The age of the β Circini system has been estimated to be in the 370–500 Myr range. We would therefore expect the V478 Lyr system to be somewhat younger than the β Circini system, but likely older than ~ 100 Myr.

Spectral typing via standard template matching leads to an L2 type. However the fit in Figure 4 is poor, with the standard not only failing to match the H band shape, but also underestimating the flux at the blue end of the spectrum (up to $\sim 1.2\mu\text{m}$). Using the Kirkpatrick et al. (2010) method, i.e. fitting only the 0.9–1.4 μm range, the best fit template is the L1 standard, but the target shows flux excess at the longer wavelength, as expected for a low surface gravity object.

If we fit V478 Lyr C with the low gravity templates defined in Allers & Liu (2013), the best fit is the $L0\beta$ standard. The fit to the H band is much more accurate, and the flux in the J band is less underestimated, but at the same time the fit to the H_2O band at $\sim 1.4\mu\text{m}$ is poorer. Given all of the above, we assign V478 Lyr C a spectral type of L1:

Filippazzo et al. (2015) derived a M_H to T_{eff} polynomial relation for young objects, but the available near-infrared photometry for V478 Lyr C is heavily contaminated by the parent star (at $\rho \sim 17$ arcsec). We computed a synthetic H -band magnitude using our flux-calibrated TripleSpec spectrum and the 2MASS H -band response curve (Cohen et al. 2003). We estimated the accuracy of our synthetic H magnitude by comparing the synthetic magnitudes obtained for the other objects observed as part of our TripleSpec run, against their measured 2MASS H (for all except HD 164507 B, since its photometry is also contaminated). The mean offset between our synthetic magnitudes and the measured ones is -0.007 mag and the 1σ dispersion around the mean is 0.44 mag. We therefore adopted 13.74 ± 0.44 mag as our synthetic measurement, and obtain $T_{\text{eff}} = 1740 \pm 130$ K for V478 Lyr C as a result. Linear interpolation of the BT-Settl isochrones for solar metallicity in the age range 0.10 – 0.37 Gyr gives a mass for this object in the range 10–28 M_{Jup} , straddling the deuterium fusion mass limit.

We determined L_{bol} for V478 Lyr C following the same procedure described in Section 4.1. The best fit model has $T_{\text{eff}} = 1800$ K, $\log g = 5.0$, and solar metallicity. The $\log g = 5.0$ is somewhat higher than one might expect, given the age of the system, and the fact that this object shows signs of youth. The radius resulting from the best-fit scaling factor is $1.31 R_{\text{Jup}}$ and the bolometric luminosity is

Table 3. Summary of atmospheric and evolutionary parameters for HD 164507 A.

Ref.	T_{eff} (K)	$\log g$ (cm s^{-2})	[Fe/H] (dex)	ξ_t (km s^{-1})	Instrument	$v \sin i$ (km s^{-1})	Age (Gyr)	Mass (M_{\odot})
1	5650 ± 40	3.93 ± 0.06	0.19 ± 0.03	...	HIRES	2.9 ± 0.5	$4.2^{+1.7}_{-1.2}$	$1.36^{+0.17}_{-0.15}$
2	...	$3.83^{+0.03}_{-0.02}$	$4.04^{+0.2}_{-0.4}$	$1.328^{+0.048}_{-0.018}$
3	...	3.78 ± 0.02	3.67 ± 0.13	1.32 ± 0.02
4	5580 ± 20	3.98 ± 0.01	0.12 ± 0.02	1.08 ± 0.01	SOPHIE	1.02 ± 0.23	3.55 ± 0.19	1.33 ± 0.03
5,6	5534 ± 5	3.66 ± 0.02	0.13 ± 0.01	1.04 ± 0.04	HRS	2.28 ± 0.64	$3.162^{+0.015}_{-0.014}$	1.440 ± 0.004
7	5540 ± 60	3.72	0.03 ± 0.07	1.54	Sandiford	5.0	$3.20 - 5.32$	$1.17 - 1.37$
8,9	5560^{+110}_{-60}	3.5	0.2	...	<i>Gaia</i>

References: 1-Valenti & Fischer (2005); 2-Takeda et al. (2007); 3-Maldonado et al. (2013); 4-Jofré et al. (2015); 5-Niedzielski et al. (2016); 6-Deka-Szymankiewicz et al. (2018); 7-Luck (2017); 8-Andrae et al. (2018); 9-Sartoretti et al. (2018).

Table 4. Spectral indices and pseudo-equivalent widths for HD 164507 B, V478 Lyr C, CD-28 8692 B, and LT UMa B.

Index	HD 164507 B	V478 Lyr C	CD-28 8692 B	LT UMa B	Ref.
H ₂ O	1.20 ± 0.01	1.23 ± 0.01	1.28 ± 0.03	1.16 ± 0.02	1
H ₂ OD	0.915 ± 0.008	0.958 ± 0.006	0.88 ± 0.02	1.07 ± 0.02	2
H ₂ O-1	0.626 ± 0.004	0.648 ± 0.006	0.63 ± 0.01	0.71 ± 0.01	3
H ₂ O-2	0.850 ± 0.009	0.841 ± 0.006	0.84 ± 0.02	0.94 ± 0.02	3
FeH _z	1.12 ± 0.07	1.34 ± 0.07	1.2 ± 0.2	1.2 ± 0.1	4
FeH _J	1.16 ± 0.02	1.22 ± 0.02	1.23 ± 0.07	1.22 ± 0.04	4
VO _z	1.18 ± 0.01	1.13 ± 0.02	1.17 ± 0.03	1.10 ± 0.02	4
KI _J	1.158 ± 0.006	1.157 ± 0.008	1.19 ± 0.02	1.12 ± 0.01	4
H-cont	0.931 ± 0.005	0.910 ± 0.005	0.92 ± 0.02	0.90 ± 0.01	4
H ₂ O- <i>J</i>	0.882 ± 0.005	0.999 ± 0.006	0.66 ± 0.01	0.93 ± 0.02	5
H ₂ O- <i>H</i>	0.851 ± 0.004	0.812 ± 0.004	0.79 ± 0.01	0.88 ± 0.01	5
H ₂ O- <i>K</i>	1.008 ± 0.006	1.036 ± 0.005	0.98 ± 0.01	1.14 ± 0.01	5
CH ₄ - <i>J</i>	0.853 ± 0.004	0.875 ± 0.005	0.99 ± 0.01	0.91 ± 0.01	5
CH ₄ - <i>H</i>	1.048 ± 0.004	1.142 ± 0.004	1.05 ± 0.01	1.020 ± 0.009	5
CH ₄ - <i>K</i>	1.018 ± 0.005	1.036 ± 0.003	1.042 ± 0.009	1.046 ± 0.009	5
<i>K</i> / <i>J</i>	0.456 ± 0.002	0.492 ± 0.002	0.380 ± 0.004	0.356 ± 0.004	5
<i>H</i> -dip	0.484 ± 0.002	0.502 ± 0.002	0.486 ± 0.006	0.487 ± 0.004	6
Line	HD 164507 B (Å)	V478 Lyr C (Å)	CD-28 8692 B (Å)	LT UMa B (Å)	Ref.
Na I 1.138 μm	10.3 ± 0.3	9.6 ± 0.3	8.6 ± 0.7	7.7 ± 0.6	4
K I 1.169 μm	6.0 ± 0.3	5.5 ± 0.3	8.0 ± 0.7	2.8 ± 0.5	4
K I 1.177 μm	6.9 ± 0.2	8.2 ± 0.3	11.0 ± 0.6	3.9 ± 0.4	4
K I 1.244 μm	5.3 ± 0.2	5.0 ± 0.3	6.9 ± 0.7	5.4 ± 0.5	4
K I 1.253 μm	5.0 ± 0.2	4.9 ± 0.2	6.7 ± 0.6	4.4 ± 0.5	4

References: 1-Allers et al. (2007); 2-McLean et al. (2003); 3-Slesnick et al. (2004); 4-Allers & Liu (2013); 5-Burgasser et al. (2006)
6-Burgasser et al. (2010).

$\log_{10}(L_{\text{bol}}/L_{\odot}) = -3.33^{+0.26}_{-0.78}$. The best fit model can be seen in Figure 5. The overall fit is good, with the model only slightly underpredicting the flux at the shortest wavelength ($\lambda < 1.2 \mu\text{m}$) but that is the region of lowest signal-to-noise-ratio.

Oh et al. (2017) found the SB1 primary to form a very wide co-moving pair with the G6V HD 171067, with a projected separation of ~ 8 pc. The Oh et al. (2017) analysis however did not take into account radial velocity (RV). The measured system RV for V478 Lyr AB is $-25.2 \pm 4.8 \text{ km s}^{-1}$ (Nordström et al. 2004), and is discrepant from the RV of HD 171067 ($-46.197 \pm 0.002 \text{ km s}^{-1}$; Soubiran et al. 2013). As a result, the G6V is unlikely to be associated with the V478 Lyr triple system.

V478 Lyr ABC joins the rank of triple systems consisting of a spectroscopic binary with a wide, low-mass tertiary

component (see Allen et al. 2012, and references therein). These systems are precious for testing formation simulations of very close separation binaries, which require a mechanism to draw angular momentum away from an already close pair of objects. One proposed mechanism is through three-body interactions with cool dwarfs (see e.g. Sterzik & Durisen 2003; Delgado-Donate et al. 2004; Umbreit et al. 2005), and a key observable to test such scenario is the fraction of tight spectroscopic binaries that have a wide additional companion. Towards this goal, V478 Lyr AB was among the stars targeted by Allen et al. (2012), who conducted a deep near-infrared survey looking for low-mass tertiary components around 118 known spectroscopic binaries within 30 pc of the Sun. However, V478 Lyr C was missed probably because of the combination of its tight angular separation from the binary (17.05 arcsec, close to the Allen et al. 2012 survey limit

of 10–15 arcsec), the large magnitude difference between SB1 primary and L dwarf companion, and the large contamination by reddened background sources resulting from its proximity to the Galactic plane ($b = 10.1$ deg).

Finally, the estimated orbital period for this system is $\gtrsim 8,000$ yr, despite this being the most favorable configuration among the seven systems presented here – i.e. a relatively massive primary, with a relatively tight separation, and assuming a face-on circular orbit. If instead we assume the wide L1: companion is coplanar with the SB1, i.e. that the inclination angle is 67 ± 12 deg, then the orbital period would be $\sim 9,700$ yr. In either case, no dynamical mass measurement is possible for the UCD. The other systems presented here have even longer estimated orbital periods.

4.3 CD–28 8692 AB

The primary is a slightly metal poor K5 V star. It has been monitored with HARPS for planets by Sousa et al. (2011), who found no evidence for RV variations. Sousa et al. (2011) also used the HARPS spectra to determine atmospheric parameters, and obtained $T_{\text{eff}} = 4799 \pm 90$ K, $\log g = 4.43 \pm 0.18$, and $[\text{Fe}/\text{H}] = -0.22 \pm 0.06$ dex. They then estimated a mass of $0.715 \pm 0.014 M_{\odot}$ for the star using the measured atmospheric parameters and the Padova isochrones. Adibekyan et al. (2012) used the atmospheric parameters estimated by Sousa et al. (2011) and the HARPS spectra to measure detailed abundances of 12 chemical species, with typical precision in the 0.035 – 0.260 dex range.

Later, Delgado Mena et al. (2015) used the HARPS data to estimate atmospheric parameters and combined them with the Li I abundance to infer an age of 4.48 Gyr for this star.

The *Gaia* DR2 effective temperature for this star is 4742^{+138}_{-116} K (Andrae et al. 2018), while the best-fit template used for radial velocity measurement has $T_{\text{eff}} = 4750$ K, $\log g = 4.5$, $[\text{Fe}/\text{H}] = -0.2$ dex (Sartoretti et al. 2018). All *Gaia* DR2 values are in good agreement with the literature measurements.

The companion presented here is classified as L2, with a projected separation of 2026 au (50.91 arcsec). The L2 template is a good fit to the spectrum of the target, with the exception of a slightly suppressed K band (typical of metal-poor and high surface gravity dwarfs; Burgasser et al. 2008; Zhang et al. 2017), and a flux excess at $\sim 1.3 \mu\text{m}$. Scatter in the strength of the $\sim 1.3 \mu\text{m}$ peak among objects of a given spectral type has been observed before (Cruz et al. 2018). The Kirkpatrick et al. (2010) method yielded a very different classification of L6. While the L6 template does indeed provide a slightly better fit to the J band reducing the over-luminosity at $\sim 1.3 \mu\text{m}$, the target is much bluer than the L6 standard at longer wavelength. Low metallicity L dwarfs are indeed slightly bluer compared to their solar metallicity counterparts, but this system is only slightly metal poor, and therefore a large suppression of the H - and K -band flux is unlikely. Moreover, the absolute G magnitude for CD-28 8692 B is 17.406 ± 0.004 mag, which is consistent with the median value for L2s (17.24 ± 0.41 mag; Smart et al. 2019), but nearly two magnitudes over-luminous compared to typical L6s (19.25 ± 0.60 mag; Smart et al. 2019). Therefore, we retain a classification of L2 for this object.

Somewhat counterintuitively, the spectral indices for

CD-28 8692 B are consistent with an INT-G classification. This is unexpected, since a relatively old, metal-poor object should exhibit surface gravity typical of standard field L dwarfs, or at most slightly higher. The transition between INT-G and FLD-G however is not very sharp, and scatter around the dividing line has been previously noted (Martin et al. 2017). The unusual metallicity of the CD-28 8692 AB system further affects the reliability of the gravity classification, as first noticed by Aganze et al. (2016) for the M9.5 companion to the metal poor M1 V GJ 660.1A ($[\text{Fe}/\text{H}] = -0.63 \pm 0.06$ dex). We therefore conclude that our INT-G classification for CD-28 8692 B is incorrect.

The solar metallicity BT-Settl isochrones at $T_{\text{eff}} = 1960 \pm 29$ K (as given by the Filippazzo et al. 2015 polynomial relations) and age = 4.48 Gyr gives a mass of $\sim 70 M_{\text{Jup}}$. Although the system is slightly metal poor, we cannot use the publicly available BT-Settl isochrones for low metallicity ($[\text{Fe}/\text{H}] = -0.5$ dex), since they do not extend below $75 M_{\text{Jup}}$ and $T_{\text{eff}} \sim 3000$ K.

We determined L_{bol} for CD-28 8692 B following the same procedure described in Section 4.1. The best fit model has $T_{\text{eff}} = 1800$ K, $\log g = 5.0$, and solar metallicity. We determine a radius of $0.87 R_{\text{Jup}}$, and $\log_{10}(L_{\text{bol}}/L_{\odot}) = -3.688^{+0.047}_{-0.053}$. The best fit model is shown in Figure 5. The model fit is of good quality, the main discrepancies being in the blue wing of the H band (the model underpredicting the observed flux) and at $\sim 1.3 \mu\text{m}$, where the model does not correctly reproduce the sharp observed peak (see above).

4.4 2MASS J23253550+4608163 + 2MASS J23253519+4608098

2MASS J23253550+4608163 is over-luminous compared to objects of similar $G - G_{\text{RP}}$ colour and spectral type. Typical M8 dwarfs have $M_G = 15.24 \pm 0.63$ mag (see GUCDS II), while our target has $M_G = 12.850 \pm 0.004$ mag⁶. The over-luminosity cannot be explained by unresolved binarity alone, since an equal-mass binary would at most be 0.75 mag over-luminous, while the target is almost 2.4 mag over-luminous. Young objects can also be redder and over-luminous compared to field-age objects. However, 2MASS J23253550+4608163 does not show any indication of youth in its near-infrared spectrum (see Figure 3, middle panel) and its kinematics are inconsistent with membership to any of the young moving groups using the BANYAN Σ on-line tool⁷ (Gagné et al. 2018). Contamination by a background object could be another possibility, and this source is indeed flagged as duplicate (`duplicated_source` = 1), however the background object would need to have the $G - G_{\text{RP}}$ colour of a late-M dwarf, since the $G - G_{\text{RP}}$ colour of 2MASS J23253550+4608163 is in line with the median colour of M8 dwarfs (1.592 ± 0.005 mag vs. 1.61 ± 0.95 mag, see GUCDS II). External photometry from 2MASS, PanSTARRS-1 and AllWISE does not show evidence of contamination nor peculiar colours, but all absolute magnitudes are similarly over-luminous when compared with M8 dwarfs.

⁶ Absolute magnitudes throughout this paper are computed using $1/\varpi$ as the distance, since for all targets $\varpi/\sigma_{\varpi} > 10$.

⁷ <http://www.exoplanetes.umontreal.ca/banyan/banyansigma.php>

An indication of possible problems is the relatively large goodness-of-fit (`astrometric_gof_al`) of 132 (cf. the mean value of 5.2 ± 2.6 for objects in GUCDS II), which may indicate that the parallax for this source is spuriously large. The companion, 2MASS J23253519+4608098, does not show any sign of peculiarity, neither photometric nor spectroscopic. This could therefore be an unfortunate case of chance alignment, with 2MASS J23253550+4608163 being a background M dwarf whose spurious astrometry is consistent, by chance, with being a companion to 2MASS J23253519+460898. The astrometry for 2MASS J23253519+46089 would instead be correct. The chance of such an unfortunate alignment is however extremely low, given the tight separation of the pair on the sky ($7.24''$). We therefore have no conclusive explanation for the overluminosity of this object.

We determined L_{bol} for both components of this system following the same procedure described in Section 4.1. The best fit model for the A component has $T_{\text{eff}} = 2400$ K, $\log g = 5.0$, and $[\text{Fe}/\text{H}] = +0.5$ dex. The radius is $3.14 R_{\text{Jup}}$ (c.f. model-predicted value of $2.33 R_{\text{Jup}}$), which is unusually large for an ultra-cool dwarf, but probably a consequence of the overluminosity discussed above. The result is $\log_{10}(L_{\text{bol}}/L_{\odot}) = -1.928^{+0.026}_{-0.027}$.

The best fit model for the B component has $T_{\text{eff}} = 1800$ K, $\log g = 5.5$, and solar metallicity. The radius corresponding to the best-fit scaling factor is $R = 1.39 R_{\text{Jup}}$ which is somewhat large for an object with this temperature and surface gravity (the BT-Settl models predict $R \sim 0.9 R_{\text{Jup}}$). The bolometric luminosity is $\log_{10}(L_{\text{bol}}/L_{\odot}) = -3.265^{+0.053}_{-0.060}$. The best fit models for both components are shown in Figure 6. The fit to the spectrum of 2MASS J23253550+4608163 is overall poor. The model appears too blue compared to the observed spectrum with the flux at $\lambda < 1.3\mu\text{m}$ being overestimated and the flux in the *K* band being underestimated. The shape of the *H* band is also poorly reproduced, with the model having a more pronounced peak, while the observed spectrum appears flatter. The fit to the L dwarf component, 2MASS J23253519+4608098, is good, with the model only slightly underpredicting the flux at $\lambda < 1.25\mu\text{m}$.

4.5 2MASS J01390902+8110003 + 2MASS J01385969+8110084

With a projected separation of 959 au, this system is to our knowledge the widest L+L dwarf binary known to date.

The primary is an L1 based on the template fitting to the whole spectrum, while a fit to the *J* band alone results in a significantly earlier spectral type, M8. The discrepancy is mostly driven by the slightly overluminous blue end of the TripleSpec spectrum ($\lambda < 1.1\mu\text{m}$, see Figure 2). The L1 standard gives a good fit to the overall spectrum except for this wavelength range, which is however also the lowest signal-to-noise-ratio portion of the spectrum. On the other hand, the M8 template reproduces better this part of the spectrum, but starts to diverge from the observations at wavelength longer than $\sim 1.3\mu\text{m}$, with the target being overall redder than the template. While in principle this could be evidence of youth, the morphology of the *H* band, and the depth of the Na I and K I absorption lines suggest that the object is not particularly young. We assume a spectral type of L1

for this object in the rest of the analysis. The companion is classified as L2 by both methods.

Various authors have focused on the identification of wide low-mass binaries. Recent examples include SLoW-PoKES (Sloan Low-mass Wide Pairs Of Kinematically Equivalent Stars; Dhital et al. 2010), Baron et al. (2015), and Gálvez-Ortiz et al. (2017). Extremely wide low mass binaries do exist, with separations out to tens of thousands of au, and are found in young clusters and moving groups (see e.g. GUCDS II, Alonso-Floriano et al. 2015) as well as in the field (Caballero 2012; Caballero & Montes 2012; Caballero et al. 2012, and Dhital et al. 2010). These systems are rare, with an estimated fraction of wide low-mass binaries in the field of 1–2% (Burgasser et al. 2009). Their paucity may be explained via Galactic dynamical evolution, with subsequent stellar encounters in the Galactic disk progressively increasing the separation between the low-mass binary components, eventually leading to its dissolution (Weinberg et al. 1987). This sets a hard lower limit on the binding energy (see e.g. Burgasser et al. 2003; Caballero 2009).

However rare, these systems pose a challenge to the formation models of low-mass stars and brown dwarfs. In particular, Kouwenhoven et al. (2010, 2011) argued that systems with separation > 1000 au are unlikely to have been formed as primordial binaries (since their orbital separation would be comparable to the size of an embedded cluster), but instead originated during the cluster dissolution process. Dhital et al. (2010) observed a bimodal binary separation (also observed by Kouwenhoven et al. 2010), suggesting the presence of two populations, one old and tightly bound, and another young and weakly bound, recently formed and unlikely to survive more than a few Gyr.

For us to determine how strongly bound this system is, we need to constrain the mass of the components. The spectra, presented in Figure 2, do not present any obvious peculiarity, and both give a good fit to the standard templates. We can therefore reasonably assume that these two L dwarfs are of solar metallicity, and with age > 0.37 Gyr (following the same reasoning used in Section 4.2). We estimate the effective temperature for the two components using the Filippazzo et al. (2015) polynomial relation, and obtain 2100 ± 29 K and 1960 ± 29 K for the L1 and L2, respectively. Given these temperatures, interpolation of the BT-Settl isochrones in the 0.37 – 13 Gyr range gives a mass of $44 - 82 M_{\text{Jup}}$ and $42 - 80 M_{\text{Jup}}$, respectively, corresponding to a total system mass in the $0.08 - 0.15 M_{\odot}$ range. The corresponding binding energy for the pair is $3 \times 10^{33} < |U_g^*| < 1 \times 10^{34} J$, just above the $|U_g^*| > 10^{33} J$ limit proposed by Caballero (2009).

We can finally estimate how long the 2MASS J01390902+8110003 + 2MASS J01385969+8110084 system is likely to survive stellar encounters in the Galactic disk, using the method described in Dhital et al. (2010). Rearranging their equation 18, and assuming a lower limit on the total mass for this system of $0.08 M_{\odot}$, we find that the expected lifetime would be > 22 Gyr. Alternatively, we can compute the maximum separation for a binary of given total mass to remain bound for at least 10 Gyr, rearranging equation 28 from Weinberg et al. (1987) and following their assumption of an average Galactic stellar density of 0.16 pc^{-3} , an average stellar mass of $0.7 M_{\odot}$, and a relative velocity for the stellar encounters of $\sim 20 \text{ km s}^{-1}$. We find the

maximum separation for a system of total mass $> 0.08 M_{\odot}$ to be $> 1.5 \times 10^3$ au. The system is therefore bound.

We determined L_{bol} for both components of the system following the same procedure described in Section 4.1. The best fit model for component A has $T_{\text{eff}} = 1950$ K, $\log g = 5.5$, and solar metallicity. We determine a radius of $2.16 R_{\text{Jup}}$ and $\log_{10}(L_{\text{bol}}/L_{\odot}) = -2.753^{+0.029}_{-0.031}$. The radius is unusually large, and inconsistent with the model-predicted radius for an object of such atmospheric properties ($1.14 R_{\text{Jup}}$).

The best fit model for the B component has $T_{\text{eff}} = 1800$ K, $\log g = 5.0$, and solar metallicity. The resulting radius is $1.58 R_{\text{Jup}}$ and $\log_{10}(L_{\text{bol}}/L_{\odot}) = -3.158^{+0.034}_{-0.037}$. The radius is once again unusually large, and even more inconsistent with the model-predicted radius for an object of such atmospheric properties ($0.91 R_{\text{Jup}}$). The best fit models for both components can be seen in Figure 6. The fit to the L1 (2MASS J01390902+8110003) is overall good, while the fit to the L2 (2MASS J01385969+8110084) is of slightly lower quality. Main discrepancies are an overall underestimated flux in the blue wing of the H band, as well as in the K band and at $\sim 1.3 \mu\text{m}$.

4.6 2MASS J18392917+4424386 + 2MASS J18392740+4424510

This is a very wide (811 au) M+L binary, akin to the 2MASS J01390902+8110003 + 2MASS J01385969+8110084 system.

The primary is the only previously known UCD discussed in this paper, and was classified M9 V using IRTF/SpeX spectroscopy in [Bardalez Gagliuffi et al. \(2014\)](#). The TripleSpec spectrum for the companion is presented in Figure 2, and does not present any obvious peculiarity. We classify it as L2 via template matching.

Following the same method described above, we estimate the T_{eff} for the two components to be 2400 ± 29 K and 1960 ± 29 K respectively, leading to masses of $49 - 88 M_{\text{Jup}}$ and $42 - 80 M_{\text{Jup}}$. The binding energy of the system is therefore $4 \times 10^{33} < |U_g^*| < 1 \times 10^{34}$ J. The expected lifetime (computed using the same procedure described in Section 4.5) is > 28 Gyr and the separation limit $> 1.6 \times 10^3$ au. The system is therefore bound.

We determined L_{bol} for the L dwarf following the same procedure described in Section 4.1. The best fit model has $T_{\text{eff}} = 1800$ K, $\log g = 5.5$, and solar metallicity. We determine a radius of $1.19 R_{\text{Jup}}$ and $\log_{10}(L_{\text{bol}}/L_{\odot}) = -3.440^{+0.042}_{-0.046}$. The best fit model is presented in Figure 5.

4.7 LT UMa AB

LT UMa is a variable star of BY Dra type, with an amplitude of 0.03 mag (no period listed) in The International Variable Star Index⁸, based on 11 observations by [Strassmeier et al. \(2000\)](#).

The companion was first identified by [Pinfield et al. \(2006\)](#) based on motion and colour, but no spectroscopy was presented there. The Washington Double Star Catalog lists the pair as WDS J08448+5532. The spectral types are

reported as “K0 III+L?”, following the primary classification presented in [Yoss \(1961\)](#) and the companion estimated spectral type derived in [Pinfield et al. \(2006\)](#). The primary was however reclassified as K0 V in [Strassmeier et al. \(2000\)](#) and [Tsvetkov et al. \(2008\)](#).

[Strassmeier et al. \(2000\)](#) determined the effective temperature for LT UMa using the *B* and *V* magnitudes taken from the Tycho catalogue ([Høg et al. 1997](#)), and the *B*–*V* calibration from [Flower \(1996\)](#) to obtain $T_{\text{eff}} = 5290$ K. More recently [Stevens et al. \(2017\)](#) combined optical and near-infrared photometry, and derived $T_{\text{eff}} = 5324 \pm 26$ K. They combined this photometric temperature with the parallax from *Gaia* DR1 ([Gaia Collaboration et al. 2016b](#); [Lindgren et al. 2016](#)) and estimated the angular diameter, finding $\theta = 174.5 \pm 1.9 \mu\text{as}$. [Stassun et al. \(2018\)](#) combined literature photometry, *Gaia* DR2 astrometry, and various colour- T_{eff} , T_{eff} -radius, and T_{eff} -mass empirical relations to determine the basic properties of LT UMa. They found $T_{\text{eff}} = 5351$ K, $\log g = 4.51 \pm 0.28$, $R_* = 0.88 \pm 0.11 R_{\odot}$, and $M_* = 0.92 \pm 0.12 M_{\odot}$. *Gaia* DR2 quotes $T_{\text{eff}} = 5342^{+92}_{-58}$ K, and the best-fit template used for radial velocity measurement has $T_{\text{eff}} = 5250$ K, $\log g = 4.5$, and $[\text{Fe}/\text{H}] = 0.0$, all in good agreement with the literature values. Finally, we determined T_{eff} through SED fitting, using the Virtual Observatory SED Analyzer⁹ (VOSA; [Bayo et al. 2008](#)). Given its brightness and relative proximity, LT UMa has photometric data covering the full range from far-UV to mid-IR. We fit this SED with the BT-Settl models ([Allard et al. 2012b](#)), available through VOSA, and found $T_{\text{eff}} = 5300$ K. Combining our VOSA-based estimate with all the values found in the literature, we adopted $T_{\text{eff}} = 5300 \pm 50$ K. VOSA measures $\log_{10}(L_{\text{bol}}/L_{\odot}) = -0.3091^{+0.0049}_{-0.0050}$ implying a radius $R_* = 0.837 \pm 0.016 R_{\odot}$.

The primary was found to be active by [Strassmeier et al. \(2000\)](#), who measured the strength of the Ca II H and K lines. [Pace \(2013\)](#) used the [Strassmeier et al. \(2000\)](#) measurements and derived an equivalent of the S-index in the Mount Wilson scale, and then used the procedure of [Noyes et al. \(1984\)](#) to convert the S-index into R'_{HK} , and measured $\log R'_{\text{HK}} = -4.443$. We used this value together with the calibrations of [Mamajek & Hillenbrand \(2008\)](#) to estimate the age of this system. Equation 3 from [Mamajek & Hillenbrand \(2008\)](#), based on chromospheric activity, leads to an age of 0.41 Gyr. We also used the activity to Rossby number correlation from [Mamajek & Hillenbrand \(2008, their equation 7\)](#) and their recalibrated colour-dependent version of the Skumanich law ([Skumanich 1972](#)), to derive a gyrochronology age of 0.70 Gyr.

The TripleSpec spectrum of the companion is presented in Figure 3, and we classify it as M9 V via template fitting. The spectrum does not show signs of youth (i.e. low surface gravity), and the gravity-sensitive spectral indices give a classification of FLD-G. As discussed in Section 4.2, low-gravity features tend to disappear by the time the object reaches ~ 400 Myr. The absence of low-gravity features from the spectrum of LT UMa B is therefore consistent with the age of the system (0.41–0.70 Gyr) and its solar metallicity. Using the [Filippazzo et al. \(2015\)](#) relation we obtain $T_{\text{eff}} = 2395 \pm 29$ K, which implies a mass in the

⁸ <https://www.aavso.org/vsx/index.php>

⁹ <http://svo2.cab.inta-csic.es/theory/vosa/index.php>

Table 5. Summary of the inferred properties for HD 164507 B, V478 Lyr C, and CD-28 8692 B.

Name	Sp. Type	T_{eff} (K)	Age (Gyr)	[Fe/H] (dex)
HD 164507 B	L1	2100±30	3.0–5.9	0.03–0.19
V478 Lyr C	L1:	1740±60	0.1–0.37	...
CD-28 8692 B	L2	1960±30	4.5	−0.22

T_{eff} for HD 164507 B and CD-28 8692 B are computed using the spectral type to T_{eff} polynomial relations for field-age objects derived in [Filippazzo et al. \(2015\)](#), while for V478 Lyr C we used the M_H to T_{eff} polynomial relation for young objects presented in the same paper.

48 – 77 M_{Jup} range. We determined L_{bol} for the M dwarf following the same procedure described in Section 4.1. The best fit model has $T_{\text{eff}} = 2300$ K, $\log g = 5.0$, and $[\text{Fe}/\text{H}] = +0.5$ dex. The radius is 1.13 R_{Jup} , in good agreement with the model-predicted radius (1.18 R_{Jup}). The bolometric luminosity is $\log_{10}(L_{\text{bol}}/L_{\odot}) = -2.968^{+0.028}_{-0.029}$. The best fit model can be seen in Figure 5. The quality of the fit is poor. The model has a triangular-shaped H band that is not present in the target, which instead displays a flat H -band spectrum. The alkali lines in the J band are also weaker in the model compared to the observed ones.

5 COMPARISON OF L DWARF SPECTRAL FEATURES

Despite the relatively small sample size, it is nonetheless interesting to compare the spectroscopic features in our newly discovered L companions. In particular, V478 Lyr C, HD 164507 B, and CD-28 8692 B offer an interesting comparison set. With very similar spectral type (L1:, L1, and L2, respectively), but different ages and metallicity, these three objects can be used to qualitatively determine the dependence of spectral features on these parameters. Properties for these three UCDs relevant to this analysis are summarised in Table 5. Figure 8 shows the normalised IR spectra, centred around four of the main absorption features in the spectra of early L dwarfs: the Na I doublet at $\sim 1.139 \mu\text{m}$, the K I doublets at $\sim 1.173 \mu\text{m}$ and $\sim 1.248 \mu\text{m}$, and the CO band head at $2.30 \mu\text{m}$.

The alkali lines in V478 Lyr C and HD 164507 B show remarkable similarity, while those in CD-28 8692 B are deeper and broader. FeH absorption in the 1.24–1.25 μm range is also stronger in CD-28 8692 B, as expected from its age, which confirms the known trend of alkali lines and hydride bands with metallicity (see e.g. [Kirkpatrick et al. 2010](#)). Surprisingly, the CO band at 2.293 μm appears deeper in CD-28 8692 B as well, while the band at 2.322 μm is in a region of too low signal-to-noise ratio. While the strength of this CO band is relatively insensitive to changes in effective temperature in the L0–4 range ([Cruz et al. 2018](#)), blue L dwarfs and L subdwarfs have weaker CO bands than their solar-metallicity counterparts (see e.g. [Zhang et al. 2017](#)). A strong CO band has been previously observed in the blue L1 dwarf 2MASS J17561080+2815238 ([Kirkpatrick et al. 2010](#)).

Comparison of the spectral indices and equivalent

widths presented in Table 4 as a function of the age and metallicity for these three systems leads to some preliminary considerations:

- the “water-based” indices H_2O , $\text{H}_2\text{O}-J$, $\text{H}_2\text{O}-H$ and, to a lesser extent, H_2OD and $\text{H}_2\text{O}-K$ appear sensitive to metallicity – e.g. $\text{H}_2\text{O}-J = 0.659 \pm 0.013$ at $[\text{Fe}/\text{H}] = -0.22$ dex vs. $\text{H}_2\text{O}-J = 0.8819 \pm 0.0054$ at $[\text{Fe}/\text{H}] = 0.03\text{--}0.19$ dex;
- the H_2OD and $\text{H}_2\text{O}-J$ indices seem sensitive to age (i.e. surface gravity) too;
- the K I lines are sensitive to age (i.e. surface gravity) but also metallicity, becoming stronger (i.e. having larger equivalent width) as age increases, but weaker at higher metallicity. As a result, the young ($\sim 100\text{--}370$ Myr) L1: V478 Lyr C has K I lines of roughly equal strength as the older (3.0–5.9 Gyr) but metal rich L1 HD 164507 B (5.52, 8.20, 5.05, and 4.89 Å for V478 Lyr C vs. 5.97, 6.87, 5.28, and 5.03 Å for HD 164507 B).

Followup of a larger sample of benchmark L dwarfs is fundamental to better identify/quantify possible dependencies of the above spectral features on age and metallicity.

6 CONCLUSIONS

We have presented seven multiple systems discovered in *Gaia* DR2 data, identified as part of our GUCDS project. The systems presented here include an L1 companion to the G5 IV star HD 164507, an L1: companion to the RS CVn star V478 Lyr, three low-mass binaries consisting of late Ms and early Ls, an L2 companion to the metal-poor K5 V star CD-28 8692, and an M9 V companion to the young variable K0 V star LT UMa. The HD 164507 and CD-28 8692 systems are particularly important benchmarks, because the primaries are very well characterised and offer excellent constraints on the atmospheric parameters of the companion. While the HD 164507 AB system is slightly metal rich, the CD-28 8692 AB system is slightly metal poor, and therefore cover an exotic region of the parameter space, where observational constraints on theoretical models is currently scarce. The V478 Lyr ABC system is a nice addition to the sample of wide low-mass tertiary components to tight binaries, a population of crucial importance to validate formation theories for tight binaries.

We have also reported the discovery of the currently widest L+L binary known – the 2MASS J01390902+8110003 + 2MASS J01385969+8110084 system, with a projected separation of about 960 au. This system, together with the other two wide low-mass wide binaries presented here, pose an increasing challenge to models of formation and evolution of wide low-mass binaries.

A first, qualitative analysis of the sample reveals tentative correlations between spectral indices, equivalent widths, and age and metallicity for the ultra-cool dwarfs presented here. Analysis of a larger sample of benchmarks will provide stronger constraints on such correlations, and *Gaia* DR2 will play a cornerstone role in shaping our understanding of ultra-cool atmospheres.

ACKNOWLEDGEMENTS

We thank the anonymous referee for helpful suggestions that improved the quality of this paper.

We thank the staff of Palomar Observatory for successful nights of observing with TripleSpec, in particular Carolyn Heffner, Paul Nied, Joel Pearman, Kajsa Peffer, and Kevin Rykoski.

FM acknowledges support by the NASA Postdoctoral Program at the Jet Propulsion Laboratory, administered by Universities Space Research Association under a contract with NASA.

Part of this research was carried out at the Jet Propulsion Laboratory, California Institute of Technology, under a contract with NASA.

This work has made use of data from the European Space Agency (ESA) mission *Gaia* (<https://www.cosmos.esa.int/gaia>), processed by the *Gaia* Data Processing and Analysis Consortium (DPAC, <https://www.cosmos.esa.int/web/gaia/dpac/consortium>). Funding for the DPAC has been provided by national institutions, in particular the institutions participating in the *Gaia* Multilateral Agreement.

SPLAT is a collaborative project of research students in UCSD Cool Star Lab. Contributors to SPLAT have included Christian Aganze, Jessica Birky, Daniella Bardalez Gagliuffi, Adam Burgasser (PI), Caleb Choban, Andrew Davis, Ivanna Escala, Aishwarya Iyer, Yuhui Jin, Mike Lopez, Alex Mendez, Gretel Mercado, Elizabeth Moreno Hilario, Johnny Parra, Maitrayee Sahi, Adrian Suarez, Melisa Tallis, Tomoki Tamiya, Chris Theissen and Russell van Linge. This project is supported by the National Aeronautics and Space Administration under Grant No. NNX15AI75G.

This publication makes use of VOSA, developed under the Spanish Virtual Observatory project supported by the Spanish MINECO through grant AyA2017-84089.

REFERENCES

Adamczyk M., Deka-Szymankiewicz B., Niedzielski A., 2016, *A&A*, **587**, A119
 Adibekyan V. Z., Sousa S. G., Santos N. C., Delgado Mena E., González Hernández J. I., Israelian G., Mayor M., Khachatrian G., 2012, *A&A*, **545**, A32
 Aganze C., et al., 2016, *AJ*, **151**, 46
 Allard F., Homeier D., Freytag B., Sharp C. M., 2012a, in Reylé C., Charbonnel C., Schultheis M., eds, *EAS Publications Series Vol. 57*, *EAS Publications Series*. pp 3–43 ([arXiv:1206.1021](https://arxiv.org/abs/1206.1021)), doi:10.1051/eas/1257001
 Allard F., Homeier D., Freytag B., 2012b, *Philosophical Transactions of the Royal Society of London Series A*, **370**, 2765
 Allard F., Homeier D., Freytag B., 2013, *Mem. Soc. Astron. Italiana*, **84**, 1053
 Allen P. R., Burgasser A. J., Faherty J. K., Kirkpatrick J. D., 2012, *AJ*, **144**
 Allers K. N., Liu M. C., 2013, *ApJ*, **772**, 79
 Allers K. N., et al., 2007, *ApJ*, **657**, 511
 Alonso-Floriano F. J., Caballero J. A., Cortés-Contreras M., Solano E., Montes D., 2015, *A&A*, **583**, A85
 Andrae R., et al., 2018, *A&A*, **616**, A8
 Bardalez Gagliuffi D. C., et al., 2014, *ApJ*, **794**, 143
 Baron F., et al., 2015, *ApJ*, **802**, 37
 Bayo A., Rodrigo C., Barrado y Navascués D., Solano E., Gutiérrez R., Morales-Calderón M., Allard F., 2008, *A&A*, **492**, 277

Bertelli G., Bressan A., Chiosi C., Fagotto F., Nasi E., 1994, *A&AS*, **106**, 275
 Bressan A., Marigo P., Girardi L., Salasnich B., Dal Cero C., Rubele S., Nanni A., 2012, *MNRAS*, **427**, 127
 Burgasser A. J., Kirkpatrick J. D., Reid I. N., Brown M. E., Miskay C. L., Gizis J. E., 2003, *ApJ*, **586**, 512
 Burgasser A. J., Geballe T. R., Leggett S. K., Kirkpatrick J. D., Golimowski D. A., 2006, *ApJ*, **637**, 1067
 Burgasser A. J.,Looper D. L., Kirkpatrick J. D., Cruz K. L., Swift B. J., 2008, *ApJ*, **674**, 451
 Burgasser A. J., Dhital S., West A. A., 2009, *AJ*, **138**, 1563
 Burgasser A. J., Cruz K. L., Cushing M., Gelino C. R., Looper D. L., Faherty J. K., Kirkpatrick J. D., Reid I. N., 2010, *ApJ*, **710**, 1142
 Burgasser A. J., et al., 2016, in *American Astronomical Society Meeting Abstracts #227*. p. 434.08
 Burningham B., et al., 2013, *MNRAS*, **433**, 457
 Burningham B., Marley M. S., Line M. R., Lupu R., Visscher C., Morley C. V., Saumon D., Freedman R., 2017, *MNRAS*, **470**, 1177
 Burrows A., Sudarsky D., Hubeny I., 2006, *ApJ*, **640**, 1063
 Caballero J. A., 2009, *A&A*, **507**, 251
 Caballero J. A., 2012, *The Observatory*, **132**, 1
 Caballero J. A., Montes D., 2012, *The Observatory*, **132**, 176
 Caballero J. A., Genebriera J., Miret F. X., Tobal T., Cairo J., 2012, *The Observatory*, **132**, 252
 Casagrande L., Ramírez I., Meléndez J., Bessell M., Asplund M., 2010, *A&A*, **512**, A54
 Chambers K. C., et al., 2016, preprint, ([arXiv:1612.05560](https://arxiv.org/abs/1612.05560))
 Cohen M., Wheaton W. A., Megeath S. T., 2003, *AJ*, **126**, 1090
 Cruz K. L., Núñez A., Burgasser A. J., Abrahams E., Rice E. L., Reid I. N., Looper D., 2018, *AJ*, **155**, 34
 Cushing M. C., Vacca W. D., Rayner J. T., 2004, *PASP*, **116**, 362
 Cushing M. C., et al., 2008, *ApJ*, **678**, 1372
 Cutri R. M., et al., 2013, Technical report, Explanatory Supplement to the AllWISE Data Release Products
 Day-Jones A. C., et al., 2011, in Johns-Krull C., Browning M. K., West A. A., eds, *Astronomical Society of the Pacific Conference Series Vol. 448*, *16th Cambridge Workshop on Cool Stars, Stellar Systems, and the Sun*. p. 833
 Deacon N. R., et al., 2014, *ApJ*, **792**, 119
 Deka-Szymankiewicz B., Niedzielski A., Adamczyk M., Adamów M., Nowak G., Wolszczan A., 2018, *A&A*, **615**, A31
 Delgado-Donate E. J., Clarke C. J., Bate M. R., Hodgkin S. T., 2004, *MNRAS*, **351**, 617
 Delgado Mena E., et al., 2015, *A&A*, **576**, A69
 Demarque P., Woo J.-H., Kim Y.-C., Yi S. K., 2004, *ApJS*, **155**, 667
 Demarque P., Guenther D. B., Li L. H., Mazumdar A., Straka C. W., 2008, *Ap&SS*, **316**, 31
 Dhital S., West A. A., Stassun K. G., Bochanski J. J., 2010, *AJ*, **139**, 2566
 Dotter A., Chaboyer B., Jevremović D., Kostov V., Baron E., Ferguson J. W., 2008, *ApJS*, **178**, 89
 Eisenhardt P. R. M., et al., 2019, arXiv e-prints, p. [arXiv:1908.08902](https://arxiv.org/abs/1908.08902)
 Evans D. W., et al., 2018, *A&A*, **616**, A4
 Faherty J. K., et al., 2016, *ApJS*, **225**, 10
 Fekel F. C., 1988, *AJ*, **95**, 215
 Filippazzo J. C., Rice E. L., Faherty J., Cruz K. L., Van Gordon M. M., Looper D. L., 2015, *ApJ*, **810**, 158
 Flower P. J., 1996, *ApJ*, **469**, 355
 Gagné J., et al., 2018, *ApJ*, **856**, 23
 Gaia Collaboration et al., 2016a, *A&A*, **595**, A1
 Gaia Collaboration et al., 2016b, *A&A*, **595**, A2
 Gaia Collaboration et al., 2018, *A&A*, **616**, A1
 Gálvez-Ortiz M. C., Solano E., Lodieu N., Aberasturi M., 2017, *MNRAS*, **466**, 2983

- Gossage S., Conroy C., Dotter A., Choi J., Rosenfield P., Cargile P., Dolphin A., 2018, *ApJ*, **863**, 67
- Gustafsson B., Edvardsson B., Eriksson K., Jørgensen U. G., Nordlund Å., Plez B., 2008, *A&A*, **486**, 951
- Harlan E. A., Taylor D. C., 1970, *AJ*, **75**, 165
- Hastie T., Stuetzle W., 1989, *Journal of the American Statistical Association*, **84**, 502
- Herter T. L., et al., 2008, in *Ground-based and Airborne Instrumentation for Astronomy II*. Edited by McLean, Ian S.; Casali, Mark M. Proceedings of the SPIE, Volume 7014, article id. 70140X, 8 pp. (2008).. , doi:10.1117/12.789660
- Høg E., et al., 1997, *A&A*, **323**, L57
- Jofré E., Petrucci R., Saffe C., Saker L., de la Villarmois E. A., Chavero C., Gómez M., Mauas P. J. D., 2015, *A&A*, **574**, A50
- Kirkpatrick J. D., et al., 2010, *ApJS*, **190**, 100
- Kouwenhoven M. B. N., Goodwin S. P., Parker R. J., Davies M. B., Malmberg D., Kroupa P., 2010, *MNRAS*, **404**, 1835
- Kouwenhoven M. B. N., Goodwin S. P., Davies M. B., Parker R. J., Kroupa P., Malmberg D., 2011, in Qain S., Leung K., Zhu L., Kwok S., eds, *Astronomical Society of the Pacific Conference Series Vol. 451, 9th Pacific Rim Conference on Stellar Astrophysics*. p. 9
- Kurucz R. L., 1992, in Barbuy B., Renzini A., eds, *IAU Symposium Vol. 149, The Stellar Populations of Galaxies*. p. 225
- Lindgren L., et al., 2016, *A&A*, **595**, A4
- Lindgren L., et al., 2018, *A&A*, **616**, A2
- Line M. R., Teske J., Burningham B., Fortney J. J., Marley M. S., 2015, *ApJ*, **807**, 183
- Looper D. L., et al., 2008, *ApJ*, **686**, 528
- Lucas P. W., Roche P. F., Allard F., Hauschildt P. H., 2001, *MNRAS*, **326**, 695
- Luck R. E., 2017, *AJ*, **153**, 21
- Maldonado J., Villaver E., Eiroa C., 2013, *A&A*, **554**, A84
- Mamajek E. E., Hillenbrand L. A., 2008, *ApJ*, **687**, 1264
- Marocco F., et al., 2014, *MNRAS*, **439**, 372
- Marocco F., et al., 2017, *MNRAS*, **470**, 4885
- Martin E. C., et al., 2017, *ApJ*, **838**, 73
- McCarthy J. K., Sandiford B. A., Boyd D., Booth J., 1993, *PASP*, **105**, 881
- McLean I. S., McGovern M. R., Burgasser A. J., Kirkpatrick J. D., Prato L., Kim S. S., 2003, *ApJ*, **596**, 561
- Niedzielski A., Deka-Szymankiewicz B., Adamczyk M., Adamów M., Nowak G., Wolszczan A., 2016, *A&A*, **585**, A73
- Nordström B., et al., 2004, *A&A*, **418**, 989
- Noyes R. W., Hartmann L. W., Baliunas S. L., Duncan D. K., Vaughan A. H., 1984, *ApJ*, **279**, 763
- Oh S., Price-Whelan A. M., Hogg D. W., Morton T. D., Spergel D. N., 2017, *AJ*, **153**
- Pace G., 2013, *A&A*, **551**, L8
- Perruchot S., et al., 2008, in *Ground-based and Airborne Instrumentation for Astronomy II*. p. 70140J, doi:10.1117/12.787379
- Pietrinferni A., Cassisi S., Salaris M., Castelli F., 2004, *ApJ*, **612**, 168
- Pinfield D. J., Jones H. R. A., Lucas P. W., Kendall T. R., Folkes S. L., Day-Jones A. C., Chappelle R. J., Steele I. A., 2006, *MNRAS*, **368**, 1281
- Ricker G. R., et al., 2015, *Journal of Astronomical Telescopes, Instruments, and Systems*, **1**, 014003
- Saffe C., 2011, *Rev. Mex. Astron. Astrofis.*, **47**, 3
- Sartoretti P., et al., 2018, *A&A*, **616**, A6
- Saumon D., Marley M. S., 2008, *ApJ*, **689**, 1327
- Skrutskie M. F., et al., 2006, *AJ*, **131**, 1163
- Skumanich A., 1972, *ApJ*, **171**, 565
- Slesnick C. L., Hillenbrand L. A., Carpenter J. M., 2004, *ApJ*, **610**, 1045
- Smart R. L., Marocco F., Caballero J. A., Jones H. R. A., Barrado D., Beamín J. C., Pinfield D. J., Sarro L. M., 2017, *MNRAS*, **469**, 401
- Smart R. L., Marocco F., Sarro L. M., Barrado D., Beamín J. C., Caballero J. A., Jones H. R. A., 2019, *MNRAS*, **485**, 4423
- Smith L., Lucas P. W., Burningham B., Jones H. R. A., Smart R. L., Andrei A. H., Catalán S., Pinfield D. J., 2014, *MNRAS*, **437**, 3603
- Smith L. C., et al., 2015, *MNRAS*, **454**, 4476
- Smith L. C., et al., 2018, *MNRAS*, **474**, 1826
- Snedden C., 1973, *ApJ*, **184**, 839
- Soubiran C., Jasniewicz G., Chemin L., Crifo F., Udry S., Hestroffer D., Katz D., 2013, *A&A*, **552**
- Sousa S. G., Santos N. C., Israelian G., Lovis C., Mayor M., Silva P. B., Udry S., 2011, *A&A*, **526**, A99
- Stassun K. G., Corsaro E., Pepper J. A., Gaudi B. S., 2018, *AJ*, **155**, 22
- Stephens D. C., et al., 2009, *ApJ*, **702**, 154
- Sterzik M. F., Durisen R. H., 2003, *A&A*, **400**, 1031
- Stevens D. J., Stassun K. G., Gaudi B. S., 2017, *AJ*, **154**, 259
- Strassmeier K., Washuettl A., Granzer T., Scheck M., Weber M., 2000, *A&AS*, **142**, 275
- Takeda Y., Ohkubo M., Sadakane K., 2002, *Publications of the Astronomical Society of Japan*, **54**, 451
- Takeda Y., Ohkubo M., Sato B., Kambe E., Sadakane K., 2005, *Publications of the Astronomical Society of Japan*, **57**, 27
- Takeda G., Ford E. B., Sills A., Rasio F. A., Fischer D. A., Valenti J. A., 2007, *The Astrophysical Journal Supplement Series*, **168**, 297
- Tsvetkov A. S., Popov A. V., Smirnov A. A., 2008, *Astronomy Letters*, **34**, 17
- Tull R. G., 1998, in D'Odorico S., ed., *Proc. SPIE Vol. 3355, Optical Astronomical Instrumentation*. pp 387–398, doi:10.1117/12.316774
- Umbreit S., Burkert A., Henning T., Mikkola S., Spurzem R., 2005, *ApJ*, **623**, 940
- Ugren A. R., Grossenbacher R., Penhallow W. S., MacConnell D. J., Frye R. L., 1972, *AJ*, **77**, 486
- Valenti J. A., Fischer D. A., 2005, *The Astrophysical Journal Supplement Series*, **159**, 141
- Valenti J. A., Piskunov N., 1996, *A&AS*, **118**, 595
- Vogt S. S., et al., 1994, in Crawford D. L., Craine E. R., eds, *Proc. SPIE Vol. 2198, Instrumentation in Astronomy VIII*. p. 362, doi:10.1117/12.176725
- Weinberg M. D., Shapiro S. L., Wasserman I., 1987, *ApJ*, **312**, 367
- Yoss K. M., 1961, *ApJ*, **134**, 809
- Zhang Z. H., Homeier D., Pinfield D. J., Lodieu N., Jones H. R. A., Allard F., Pavlenko Y. V., 2017, *MNRAS*, **468**, 261
- da Silva L., et al., 2006, *A&A*, **458**, 609

APPENDIX A: OBSERVING LOG

This paper has been typeset from a $\text{\TeX}/\text{\LaTeX}$ file prepared by the author.

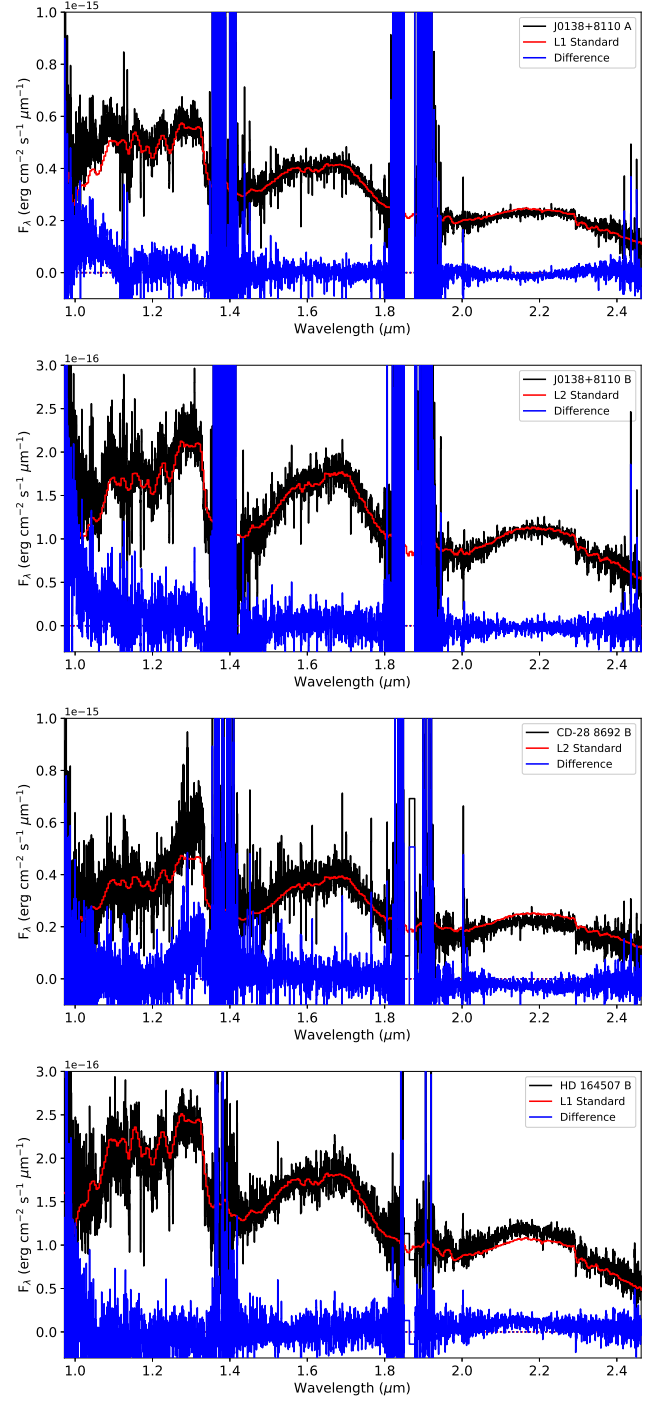


Figure 2. Spectral classification of the four UCD companions to GK stars observed with TripleSpec. In each panel we show the target spectrum (black), the best-fit template from the SpeX Prism library (red) and the difference between the two (blue). Spectral typing is done with SPLAT (Burgasser et al. 2016).

Name	Night (UT)	Exp. Time DIT (s) \times NDIT	Standard	Standard V mag	Standard Exp. Time DIT (s) \times NDIT
HD 164507 B	2018-04-28	240 \times 8	HD165029	6.42	10 \times 4
V478 Lyr C	2018-04-29	300 \times 8	HD192538	6.46	10 \times 4
CD-28 8692 B	2018-04-28	240 \times 8	HD98949	7.52	10 \times 4
2MASS J18392740+4424510	2018-04-29	300 \times 8	HD192538	6.46	10 \times 4
2MASS J01390902+8110003	2018-10-16	180 \times 4	HD8424	6.36	5 \times 4
2MASS J01385969+8110084	2018-10-16	240 \times 8	HD8424	6.36	5 \times 4
2MASS J23253550+4608163	2018-10-16	120 \times 4	HD219290	6.31	5 \times 4
2MASS J23253519+4608098	2018-10-16	300 \times 8	HD219290	6.31	5 \times 4
LT UMa B	2019-04-16	300 \times 8	HD91311	6.53	30 \times 4

Table A1. Log for the Palomar TripleSpec observations.

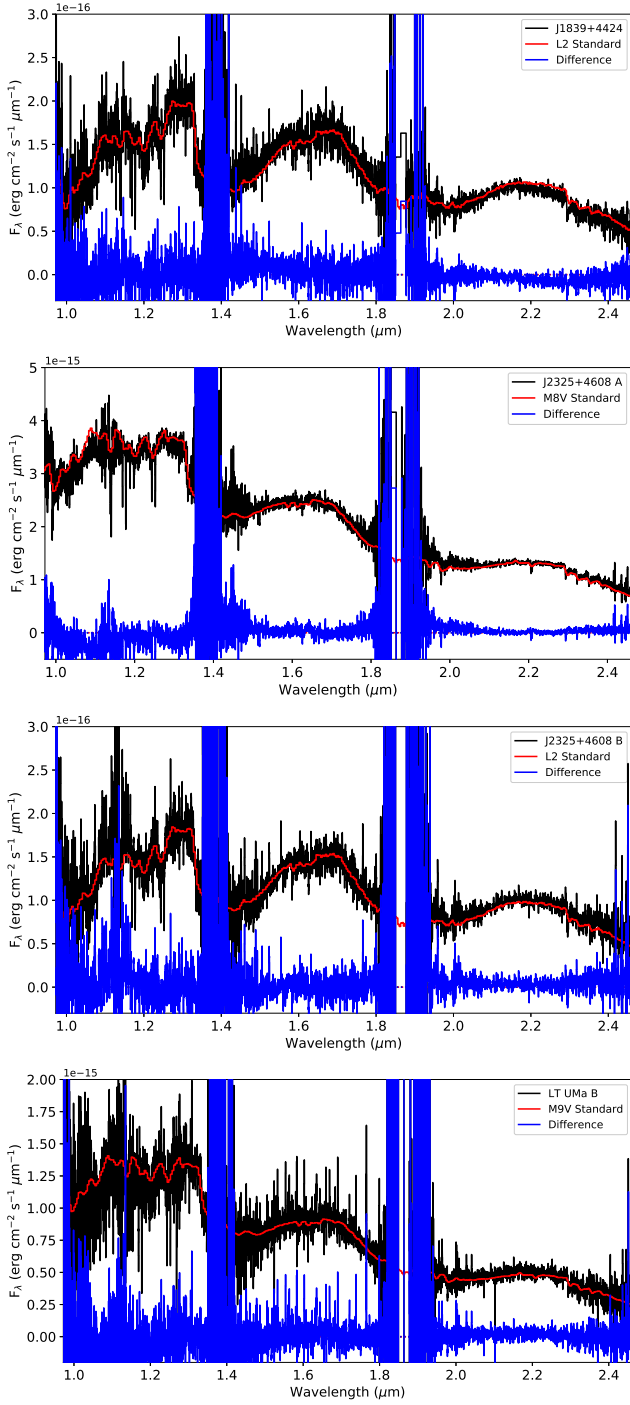


Figure 3. Same as Figure 2, but for 2MASS J18392740+4424510, 2MASS J23253550+4608163, 2MASS J23253519+4608098, and LT UMa B.

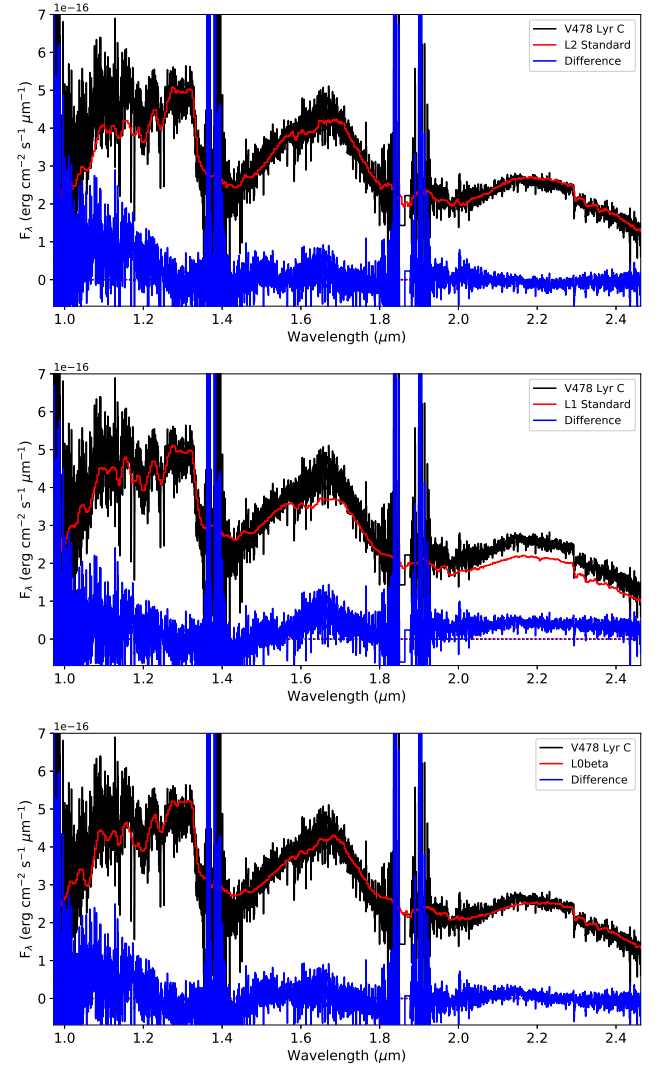


Figure 4. Spectral classification for V478 Lyr C. The top panel shows the best fit standard template fitting the whole spectrum, the middle panel shows the best fit standard template using the Kirkpatrick et al. (2010) method, while the bottom panel shows the best fit INT-G template (defined in Allers & Liu 2013). The colour-coding of spectra is the same as Figure 2.

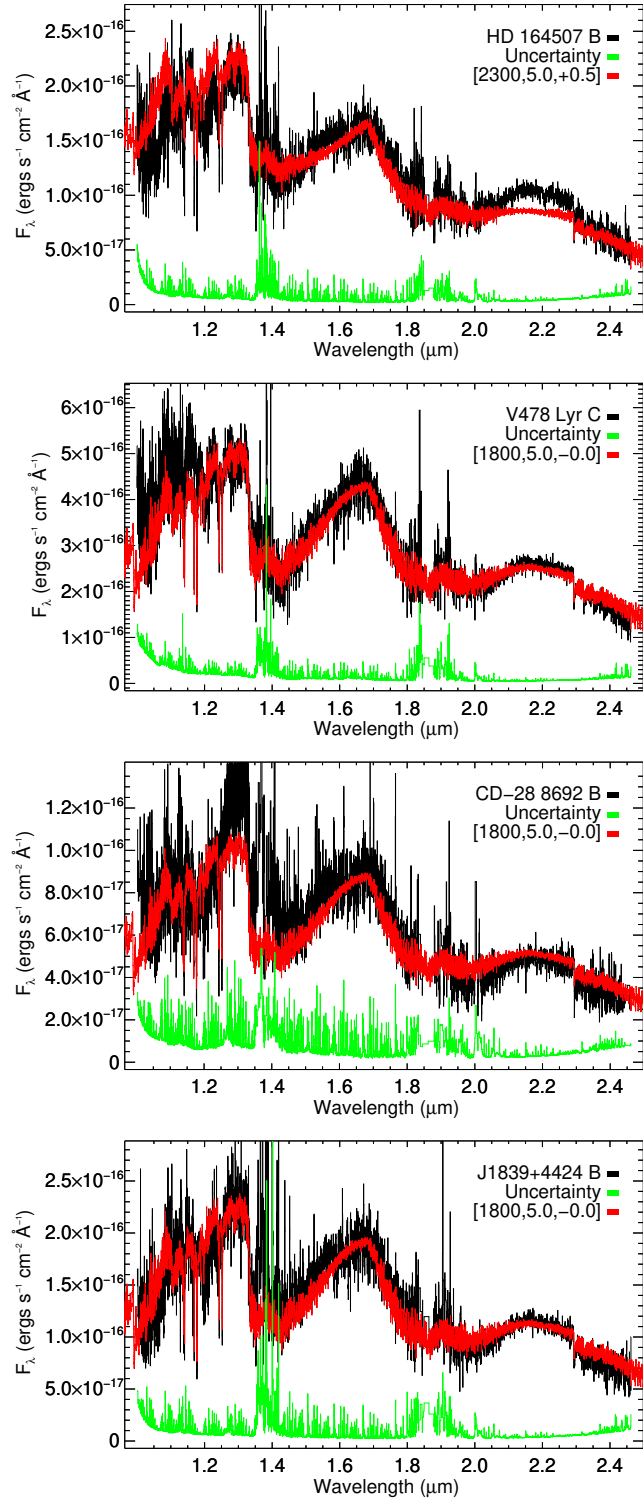


Figure 5. The spectra of HD 164507 B, V478 Lyr C, CD-28 8692 B, and 2MASS J18392740+4424510 (black) with the measured flux uncertainty (green) and the best-fit BT-Settl atmospheric model (red). The best-fit T_{eff} , $\log g$, and $[\text{Fe}/\text{H}]$ are indicated on the plot. For details on the fitting procedure, see Sections 4.1–4.7.

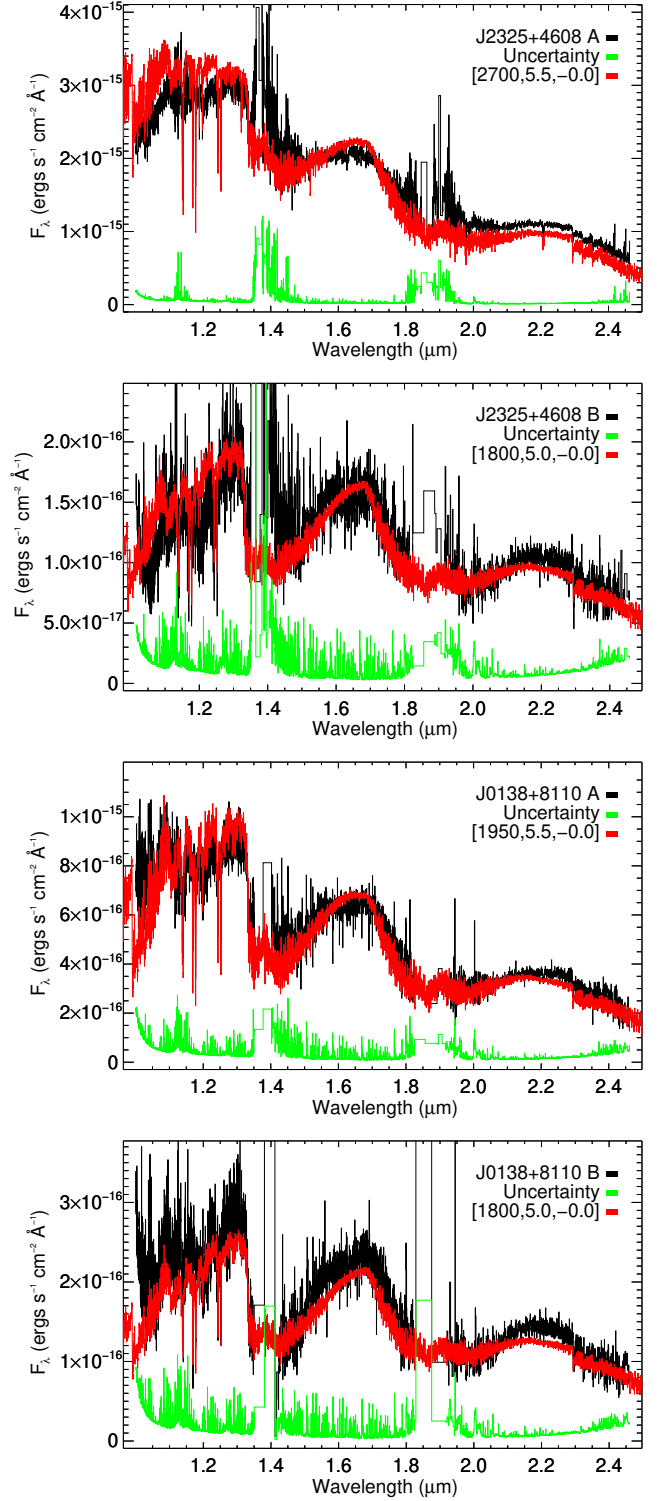


Figure 6. Same as Figure 5, but for 2MASS J23253550+4608163, 2MASS J23253519+4608098, 2MASS J01390902+8110003, and 2MASS J01385969+8110084.

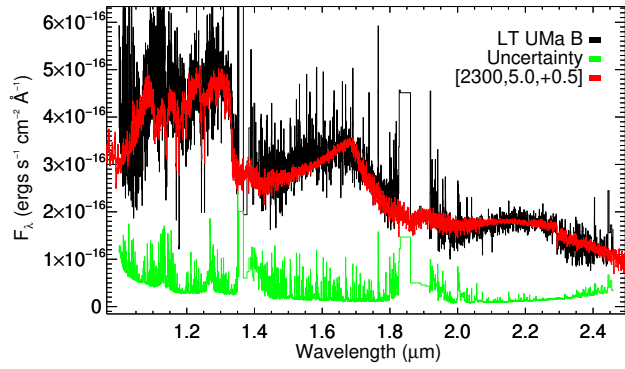


Figure 7. Same as Figure 5, but for LT UMa B.

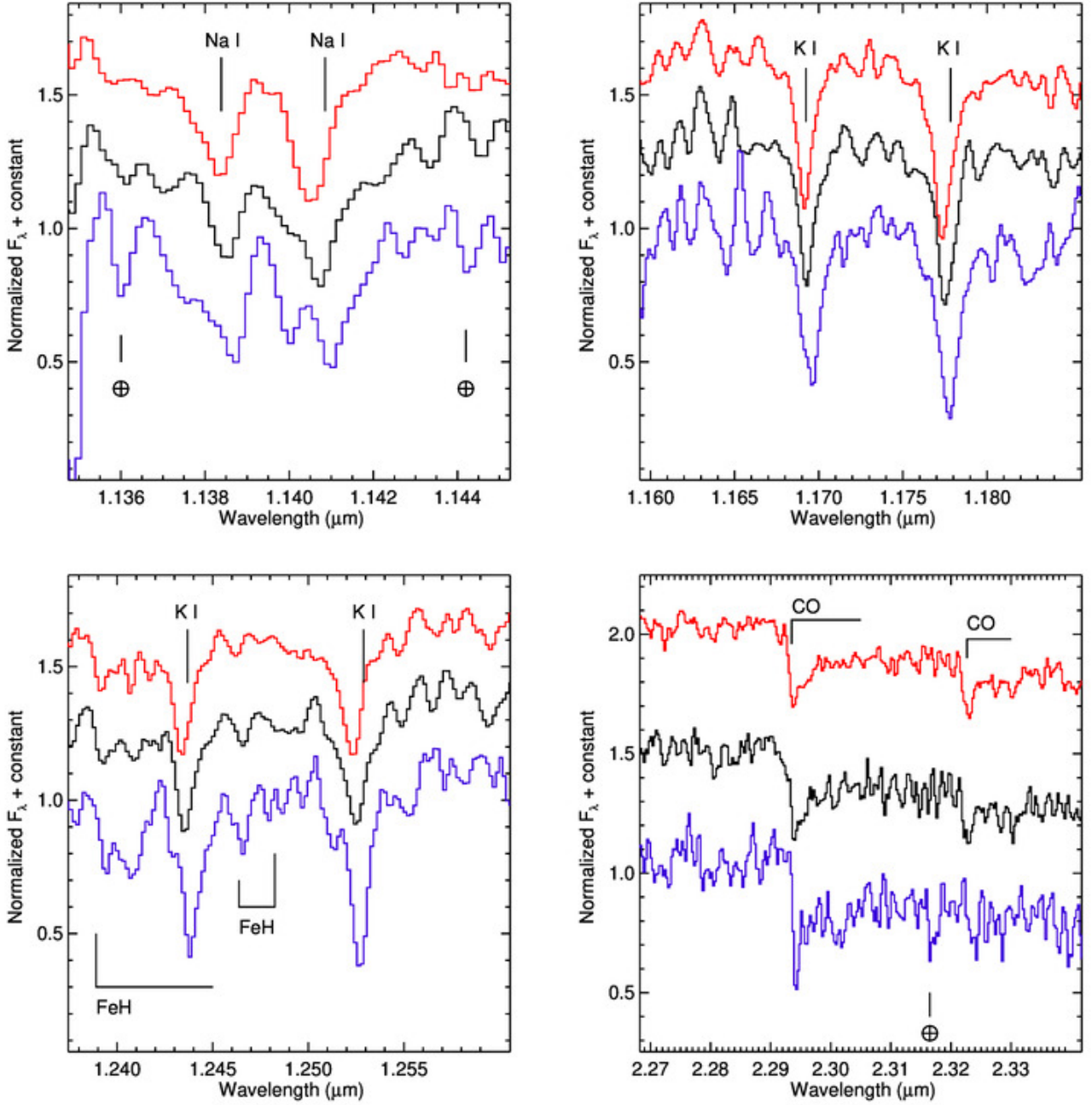


Figure 8. A direct comparison of the main absorption features in the spectra of V478 Lyr C (red), HD 164507 B (black), and CD-28 8692 B (blue). Features likely due to telluric absorption are labelled with the symbol \oplus . All spectra are smoothed down to a resolution of 3 \AA pix^{-1} to reduce the noise. The alkali lines in V478 Lyr C and HD 164507 B show remarkable similarity, while those in CD-28 8692 B are deeper and broader, confirming the known trend with metallicity (see e.g. Kirkpatrick et al. 2010). The CO band head at $2.293 \mu\text{m}$ appears deeper in CD-28 8692 B as well, while the CO band head at $2.322 \mu\text{m}$ is in a region of too low signal-to-noise-ratio.